MICRORNA: PROFILING AND FUNCTIONAL IMPLICATIONS IN CANCER AND METABOLISM

A Dissertation

Presented to

the Faculty of the Department of Biology & Biochemistry

University of Houston

—

In Partial Fulfillment

of the Requirements for the Degree

Doctor of Philosophy

—

By

Xin Wang

December 2012

MICRORNA: PROFILING AND FUNCTIONAL IMPLICATIONS IN CANCER AND METABOLISM

Xin Wang

APPROVED BY:

Dr. Xiaolian Gao, Chairperson

Dr. Amy Sater

Dr. Cecilia Williams

Dr. Changgong Liu

Dr. Mark A. Smith Dean, College of Natural Sciences and Mathematics

ACKNOWLEDGEMENTS

My special thanks first go to my advisor, Dr. Xiaolian Gao, for her guidance and support throughout my whole study. Her inspiration and encouragement made me think and work hard in the field I would like to explore. I would also like to express my gratitude to my committee members: Dr. Amy Sater, Dr. Cecilia Williams, and Dr. Changgong Liu for their invaluable suggestions to my projects during my graduate study. In addition, I would like to thank my lab members for their discussions and technical efforts on my research. Last, but certainly not least; my deepest gratitude goes to my dear parents for their constant encouragement and unconditional support in my pursuit of doctorate degree.

MICRORNA: PROFILING AND FUNCTIONAL IMPLICATIONS IN CANCER AND METABOLISM

An Abstract

Presented to

the Faculty of the Department of Biology & Biochemistry

University of Houston

—

In Partial Fulfillment

of the Requirements for the Degree

Doctor of Philosophy

—

By

Xin Wang

August 2012

ABSTRACT

MicroRNAs (miRNAs) are a class of ~22 nt short, non-coding RNAs that post-transcriptionally regulate target mRNA expression. To date, ~2,000 mature miRNAs have been identified in humans and they are estimated to regulate about 50% of human genes. miRNAs, due to their ubiquitous target distribution, contribute to diverse processes including cell development, proliferation, differentiation, apoptosis, and metabolism. Dysregulation of miRNA expression has been reported in various cancers and metabolic disorders. miRNA are also implicated in the initiation and progression of those diseases. In my dissertation, I studied the differentially expressed (DE) miRNAs upon prostaglandin E2 (PGE2) stimulation in prostate cancer cells (PC-3). Concurrently I examined mRNA expression profile of the PC-3 system and determined anticorrelated miRNA:mRNA pairs. The DE miRNAs and their putative targets were affected by the induction of PGE2. They were suggested to be involved in PGE2 dysregulated signaling pathways in PC-3 prostate cancer. In the second part of the thesis work, I identified a set of adipose-enriched miRNAs from porcine tissues samples and verified that these miRNAs were conserved in humans. Adipose-enriched miRNAs were reported to be involved in metabolism,

inflammation responses, and tumorigenesis. The analysis results of my thesis experiments suggested adipose-enriched miRNAs may have a potential role in connecting obesity, inflammation, and cancer. It is hoped that the understanding of the molecular basis in cancer and metabolic disorders on the miRNA level will provide new diagnostic targets and therapeutic targets for the diseases.

TABLE OF CONTENT

LIST OF FIGURES

LIST OF TABLES

LIST OF ABBREVIATIONS

3'-UTR	3' untranslated regions
AA	arachidonic acid
aa-aRNA	aminoallyl-labeled antisense RNA
BMI	body mass index
COX	cyclooxygenase
DE	differentially expressed
EMT	epithelial-to-mesenchymal transition
EP receptors	E-prostanoid receptors
ESCC	esophageal squamous cell carcinoma
FC	fold change
G418	geneticin
GO	gene ontology
HCC	hepatocellular carcinoma
HNSCC	neck squamous cell carcinoma
lncRNAs	long non-coding RNAs
LOWESS	locally weighted regression
miRNAs	microRNAs
mRNAs	messenger RNAs
MTT	3-(4, 5-dimethylthiazol-2-yl)-2, 5-diphenyl tetrazolium bromide
ncRNAs	non-coding RNAs

NGS	next-generation sequencing
NSAIDs	nonsteroidal anti-inflammatory drugs
nt	nucleotides
PGD2	prostaglandin D2
PGE2	prostaglandin E2
PGES	PGE2 synthase
PGF2α	prostaglandin F2 alpha
PGI2	prostacyclin I2
PGs	prostaglandins
piRNAs	PIWI-interacting RNAs
pre-miRNAs	precursors miRNAs
pri-miRNAs	primary miRNAs
qRT-PCR	quantitative reverse transcription polymerase chain reaction
RISCs	RNA-induced silencing complexes
RQ	relative quantities
rRNAs	ribosomal RNAs
SAT	subcutaneous adipose tissues
SEM	standard error of mean
sequ-seqs	sequenced sequences
snRNAs	small nuclear RNAs
snoRNAs	small nucleolar RNAs
snoRNPs	small nucleolar ribonucleoproteins

snRNAs	small nuclear RNAs
tRNAs	transfer RNAs
TXA2	thromboxane A2
VAT	visceral adipose tissues
XIST	X-inactivation specific transcript
ZEB1	zinc finger E-box-binding homeobox 1

–

Chapter 1: General Introduction

–

1.1 Eukaryotic transcriptome

1.1.1 Eukaryotic transcriptome

Upon the development of current technology, we broaden our knowledge from protein-coding RNA to transcriptome: the entire transcripts in a cell (1). A transcriptome consists of two major categories of RNA transcripts: messenger RNAs (mRNAs), which are transcribed from protein-coding genes and will further determine the sequences of amino acids in coded proteins, and non-coding RNAs (ncRNAs), which can not be translated into proteins, such as ribosomal RNAs (rRNAs), transfer RNAs (tRNAs), microRNAs (miRNAs), small nuclear RNAs (snRNAs), small nucleolar RNAs (snoRNAs), PIWI-interacting RNAs (piRNAs), and long non-coding RNAs (lncRNAs). Notably, protein-coding genomic regions and protein-coding transcripts only account for less than 1.5% to 2% of the whole genome or 5% of the transcriptome. A significant portion of genome and transcriptome (>98% and 95%, respectively) are non-coding genomic region or ncRNAs (2). Recent studies have revealed the crucial role of

ncRNAs in various aspects of cellular processes including development, proliferation, apoptosis, angiogenesis, immune responses, *etc.* (2).

1.1.2 mRNA, tRNA, and rRNA

mRNAs are RNA transcripts which encode protein products. mRNAs are transcribed from protein-coding regions of the genome (genes). The human genome contains around 23,000 to 25,000 genes identified by the Human Genome Project (www.ornl.gov/sci/techresources/Human_Genome/home.shtml). After transcription, mRNAs will go through several processing steps, including 5' cap addition, splicing, editing, and 3' polyadenylation, before they become mature and ready to be transported into cytoplasm where they are translated into proteins. The genetic information carried by mRNAs is encoded into codons consisting of three bases each. Codons determine amino acid sequences in the protein products during the translation step.

The process of translation also requires two classes of non-coding RNAs: tRNAs which recognize codons and transport corresponding amino acids to be

incorporated into the polypeptide chains, and rRNAs which comprise the protein synthesis machinery (3).

1.1.3 Other ncRNAs

ncRNAs directly function as structural, catalytic, or regulatory RNAs, instead of being designated to carry genetic "blueprint". In this dissertation, I will focus on one class of ncRNAs which is called miRNAs. They post-transcriptionally regulate target mRNA expression by complementary binding to their 3'-untranslated regions (3'-UTRs). The biogenesis and functional mechanism of miRNAs will be discussed later. Besides miRNAs, which are the most widely studied class of ncRNAs, several other classes of ncRNAs have emerged including snRNAs, snoRNAs, piRNAs, and lncRNAs (2).

1.1.3a snRNAs

snRNAs are small, highly abundant, and uridine-rich non-coding RNAs in the nucleoplasm (4) which are about 150 nt in length. They include U6, U4, and U2, which complex with small nuclear ribonucleoproteins (snRNPs) and are involved in RNA splicing, in the activity of RNA polymerase II and transcription factor, and in maintaining the telomeres (4).

1.1.3b snoRNAs

A large group of snRNAs are known as snoRNAs. They are enriched in nucleolus, which is the nuclear compartment where ribosomal RNAs are transcribed and assembled. snoRNAs have average lengths between 60 and 300 nt. They, together with corresponding protein partners, comprise the small nucleolar ribonucleoproteins (snoRNPs), which mainly function in rRNA modification including sequence-specific 2'-O-methylation and pseudouridylation. In addition to rRNA, snoRNAs are determined to post-transcriptionally modify other structural RNAs such as tRNAs and snRNAs (2, 3).

1.1.3c piRNAs

piRNAs are RNAs that associate with the PIWI subfamily of Argonaute family proteins and are of 24-30 nt in length. Argonaute family proteins are the prime components of RNA-induced silencing complexes (RISCs), which silence their targets either by cleavage and degradation or by translational inhibition. Argonaute family can be divided into Ago and PIWI subfamilies. Among them, Ago is expressed ubiquitously while PIWI is expressed within germline cells and stem cells. piRNAs and PIWI proteins function to suppress the expression of transposable elements in germline cells or impair their mobilization. Additionally, recent findings also revealed their role in regulation of DNA methylation on epigenetic level (2, 5).

1.1.3d lncRNAs

lncRNAs are non-coding RNAs with length larger than 200 nt and are identified as the largest family of ncRNAs. lncRNA dysregulation has been determined in various diseases including cancer. They are able to mediate DNA methylation by recruiting chromatin-remodeling complexes in a temporal and spatial specific manner. One example to demonstrate the role of lncRNAs is their regulation of X-chromosome inactivation in mammals. X-inactivation specific transcript (XIST), a 17kb lncRNA, recruits polycomb complex to silence one of the two X chromosomes in females (2). Meanwhile, TSIX, a complementary form of XIST, regulate XIST expression during this process. lncRNAs have emerged as a newly highlighted target for biomarker discovery and therapeutic interventions (2, 6).

1.2 miRNA

1.2.1 miRNA biogenesis and function

miRNAs are a class of ~22 nt long, non-coding RNAs that post-transcriptionally regulate target messenger RNA (mRNA) expression by binding to their 3'-UTRs (7). miRNAs are first transcribed from genomic DNA by RNA polymerase II as primary miRNAs (pri-miRNAs), which are usually long sequences with the 5' end capped and the 3' end polyadenylated. These pri-miRNAs are cleaved into approximately 60-70 nt precursors (pre-miRNAs) with a 5' phosphate and a two-nucleotide 3' overhang. Next, exportin-5 transports the pre-miRNAs, via a Ran-GTP-dependent mechanism, from the nucleus to the cytoplasm where pre-miRNAs are further processed into short double strand miRNA: miRNA* duplexes by the endonuclease *Dicer*. Mature miRNA sequences form when a helicase unwinds the miRNA: miRNA* duplex. Both miRNAs and miRNA*s are integrated into the RISCs; however, the non-functional miRNA*s are presumably degraded (8).

miRNA in the context of RISCs has the ability to complementarily pair with 3'-UTR of its target mRNA through miRNA "seed" region (typically the eight nucleotides from the second site of 5' end). The pair binding will down-regulate target mRNA expression either through transcript degradation or through translational inhibition (8).

Since its first discovery in *Caenorhabditis elegans* in 1993 by Victor Ambros and colleagues, about 2,000 miRNAs have been estimated in the human genome according to mirBase version 18.0 (accessed January 2012) and they are expected to pair and regulate a significant portion (higher than 50%) of all protein-coding genes (9). Profiling studies of miRNAs and client mRNAs suggest that miRNAs contribute dramatically to cellular and developmental processes such as cell cycle regulation, cell proliferation, differentiation, and apoptosis.

1.2.2 miRNA detection and profiling

Based on their significant role in biological functions and cellular processes, miRNA detection and profiling is drawing remarkable attention. Northern blot was

the first described method for miRNA detection. Its major limitations are RNA degradation, low sensitivity, low throughput, high time consumption (10), and that it requires previous knowledge of the miRNA sequence (11).

Three major approaches which are well established currently include: quantitative reverse transcription PCR (qRT-PCR), miRNA microarray, and miRNA sequencing (miRNA-seq) (11). For the miRNA qRT-PCR approach, in order to overcome the lack of a common sequence for reverse transcription primer binding, there are two commercially available strategies: one is enzymatic polyadenylation at 3' end of miRNAs, and the other is ligation of a universal sequence as primer binding site in reverse transcription step. The advantage of qRT-PCR is its sensitivity, specificity, and absolute quantification, while the major drawback is its low to medium throughput capacity and lack of ability for novel sequence discovery.

Microarray technology enables parallel analysis of large numbers of miRNAs on a single platform. To date, various approaches have been developed to prepare miRNA samples which will be subject to microarray detection and profiling. The

approach I used in my dissertation is based on a platform developed by LC Sciences. Its principal sample preparation steps include enzymatically catalyzed ligation of a short oligonucleotide to the 3'-OH end of miRNA using T4 RNA ligase. This is followed by hybridization to the array and staining with fluorophore-conjugated oligonucleotides that will specifically bind to the ligated short oligo. miRNA microarray has the advantage on the cost and time-consumed per sample. Limitations include non-specific hybridization, non-uniformed ligation during sample preparation, difficulty to use for absolute quantification, and the requirement of known miRNA sequences (11).

Recently developed next-generation sequencing (NGS) enables detection of both novel and known miRNAs as well as precise determination of miRNA sequences. For instance, NGS is able to distinguish isoform sequences of miRNAs which differ by one single nucleotide. Major limitations with NGS are its high cost and great request of computational aid for data analysis. Besides that, it also has sequence bias/preference related to enzymatic steps in small RNA cDNA library preparation process and mutations introduced by PCR amplification of the library (11).

The three major NGS technology providers are Roche/454, Solid from Applied Biosystems and Illumina. The NGS technology I applied in this dissertation was the Illumina platform. The pipeline of this platform includes preparation of small RNA cDNA library and subsequent massively parallel sequencing of it. Data obtained from this platform are further filtered and processed into copy number of each sequenced sequence (sequ-seqs). However, this copy number cannot be used for absolute quantification of a particular miRNA because its measurement is not independent of other miRNAs. One common approach to represent the abundance of a specific miRNA in a sample is to calculate the percentage of its reads to total reads (or total mappable reads). It is important to carefully examine the frequency distribution of miRNA reads between samples. If the distributions are at high variance, absolute quantification is not reliable (11).

miRNA detection and profiling let us determine the differentially expressed (DE) miRNAs between samples of our interest. NGS also allows us to explore the novel miRNAs in poorly studied organisms. This is the first step of miRNA quantification and functional annotation.

1.2.3 miRNA and diseases

miRNAs are so widely involved in biological progressions that miRNA dysregulation is a common feature in cancer. Based on previous studies, miRNAs can be functionally categorized as oncogenes or tumor suppressors. For example, mammalian let-7 miRNAs, in particular let-7a-2, let-7c, and let-7g, negative regulate the human proto-oncogene RAS. Down-regulation of let-7 family in lung cancers subsequently leads to aberrant cell proliferation. In this case, members of the the let-7 miRNA family act as tumor suppressor. Conversely, miR-221 and miR-222 can act as oncogenes by targeting the CDK inhibitor P27kip1 and disrupting cell cycle restriction (9).

In addition to cancer, miRNAs are involved in metabolic disorders such as type 2 diabetes, obesity, and glucose resistance. For example, miR-103/107 mediates insulin sensitivity and controls glucose homeostasis in mouse liver (12). miR-122, which is the most prevalent miRNA in liver and is conserved among multiple species, controls cholesterol accumulation in mouse liver (13). miR-143 regulates

lipid metabolism and its expression in liver is induced by obesity. Upregulated miR-143 impairs glucose homeostasis (14). miR-375 also mediates glucose regulation of insulin gene expression and β cell growth in the pancreas (15).

Aberrant expression of miRNAs is regulated by transcription factors with the same mechanism as protein-coding mRNAs. One well-reported reciprocal relationship is between miR-200 family and zinc finger E-box-binding homeobox 1 (ZEB1). ZEB1 is a transcription repressor which negatively regulates expression of the miR-200 family. In turn, miR-200 is also negatively targeting and regulating ZEB1 (16). Discovery of disease-specific miRNA signatures and the identification of miRNA targets, regulatory pathways, and related functions will benefit miRNA-based early diagnosis and therapy.

In my dissertation, I set to explore miRNA profiles and their functional implications under specific biological conditions of our interest. Chapter 2 described miRNAs that had been altered in prostate cancer cell line (PC-3) by endogenous induction of prostaglandin E2 (PGE2). We also profiled mRNAs within the same samples and performed miRNA;mRNA anticorrelation analysis.

Based on the miRNA and mRNA profile analysis, we proposed that PGE2-ZEB1-miR-200b-PLCG1 may represent one crucial axis underlying the mechanism of PGE2 in prostate cancer development and progression. In Chapter 3, I focused on adipose miRNAs and found them to be implied in obesity, inflammation, and last but not least, cancer. I systematically screened profiles of six types of adipose tissues and two types of muscle tissues obtained from pigs. From them, I determined a set of adipose-enriched miRNAs that were of high abundance only in porcine adipose tissues. Adipose-enriched miRNAs were reported to be associated with metabolism, inflammatory responses, and oncogenesis in various types of cells by previous literatures. Additionally, our miRNA pathway enrichment analysis revealed that abundant miRNAs in adipose tissues and in human breast cancer cells shared a great portion of enriched KEGG pathways. Our findings provided potential miRNA-biomarkers for prediction and prevention of obesity and inflammation. Our analysis results suggested adipose-enriched miRNAs may have a role in connecting obesity, inflammation, and cancer.

Taken together, my dissertation focused on miRNA profiling and *in silico* analysis. Elucidation of their specific profiles and functions will complement our

understanding of non-coding RNAs and the whole eukaryotic transcriptome. miRNA-based investigation and therapy development have gained increased attention. Although there are many hurdles to overcome, early clinical results shed light on our way to success.

–

Chapter 2: Integrative Analysis of MicroRNA and mRNA Profiles Revealed a Novel Regulatory Mechanism of Prostaglandin E2 (PGE2) in Prostate Cancer

–

2.1 Key words

prostaglandin E2 (PGE2), microRNA (miRNA), gene expression, integrative analysis, pathway, prostate cancer

2.2 Abstract

Prostaglandin E2 (PGE2), a 20-carbon lipid-signaling molecule, is synthesized from arachidonic acid (AA) by cyclooxygenase (COX) enzymes and PGE2 synthase enzymes (PGES). In the PGE2 autocrine loop, PGE2 interacts with the E-prostanoid receptors, EP1-4, and regulates subsequent signaling pathways. Those pathways contribute to tumorigenesis and progression via induction of cell proliferation, angiogenesis, invasion, and suppression of cell apoptosis. In this study, we investigated microRNAs (miRNAs) whose expression was disturbed by PGE2 using a prostate cancer cell line (PC-3) which stably expresses COX-2-10aa-mPGES-1 (PC-3/PGE2), a novel engineered enzyme that directly and efficiently converts AA to PGE2. Concurrently, we profiled mRNA expression within the same samples and performed an integrative miRNA:mRNA analysis.

Through this analysis, we identified significant downregulation of miR-200a and miR-200b in the PC-3/PGE2 cells, and proposed this to be a result of ZEB1 elevation. One putative downstream target of miR-200b is PLCG1, whose expression was upregulated in PC-3/PGE2 cells. Increase in PLCG1 expression activates PI3K/Akt and MAPK pathways and thereby stimulates cell proliferation, survival, and migration. Our study identified a group of miRNA:mRNA pairs whose expression profiles were coherently changed by induction of PGE2 in prostate cancer. Thus, these miRNA:mRNA pairs might be involved in PGE2-related alteration of gene expression, cell function, and signaling pathways. These miRNAs may also serve as potential therapeutic targets for the treatment of PGE2-associated cancer and inflammation.

2.3 Introduction

Prostaglandins (PGs), whose members include prostaglandin E2 (PGE2), prostaglandin D2 (PGD2), and prostaglandin F2 alpha ($PGF2_{\alpha}$), are bioactive lipids produced by the catalyzation of cyclooxygenases (COXs) and PG synthases on arachidonic acid (AA) (17-19). Once exported to the

microenvironment, PGs bind to G-protein-coupled receptors in an autocrine or paracrine manner (19). PGs were first discovered and isolated from human seminal vesicles, and were later found to be produced in nearly all tissues of human body. They mediate a wide range of physiological and cellular processes such as control of blood pressure, contraction of smooth muscle, inflammation, and cancer progression (20).

Among members of prostaglandins, PGE2 is commonly and ubiquitously produced in various types of cancer. More importantly, it is the most abundant PG found in prostate cancer (21, 22). PGE2 is produced from AA by COXs: COX-1 and COX-2, and subsequent PGE2 synthase enzymes (PGES), such as microsomal prostaglandin E2 synthase (mPGES-1, mPGES-2) and cytosolic prostaglandin E2 synthase (cPGES). COX-1 is constitutively expressed in many tissues, whereas COX-2 and mPGES-1 are both inducible in response to extracellular pro-inflammatory stimuli such as cytokines and growth factors (17, 18, 21-25). Therefore, once the expression of COX-2 and mPGES-1 are triggered by pro-inflammatory signals, they will enhance the production of their major downstream metabolite, PGE2.

PGE2 functions as a pro-inflammatory factor by interacting with its EP1-4 receptors, and thereby participates in the regulation of downstream signaling pathways in proliferation, angiogenesis, invasion, and suppression of apoptosis (17). Thus aberrant biosynthesis of PGE2 will not only cause inflammation but also contribute to cancer development and progression (17, 18, 21).

Although extensive investigations had been carried out to study the molecular basis of PGE2, to date there are no reports elucidating changes in miRNA profiles in prostate cells over-producing PGE2 or identifying anticorrelated mRNAs. Instead of manipulating exogenous synthetic PGE2 level in PC-3 cells, we applied a novel engineered hybrid enzyme COX-2-10aa-mPGES-1, which can directly and efficiently convert endogenous AA into PGE2 (28). Our results indicated that elevation of endogenous PGE2 level directly or indirectly dysregulated a group of miRNAs that could potentially perturb their target mRNA expression and corresponding cellular signaling pathways. These pathways were implied in acceleration of tumor growth, invasion, and inhibition of apoptosis. Simultaneous survey of miRNA and mRNA profiles in the same sample provided a promising way to assess the inversely correlated miRNA:mRNA pairs (29-31),

which helped us to better understand the role of miRNAs and their interplay with putative target gene expression in the prostaglandin pathway in prostate cancer.

2.4 Materials and methods

2.4.1 Materials

Media, Geneticin (G418), Lipofectamine 2000, Alexa Fluor® 3 dyes, SuperScript Indirect RNA Amplification System, and NCode™ EXPRESS SYBR® GreenER™ miRNA kits were purchased from Invitrogen (Carlsbad, CA). FBS was purchased from Sigma (St. Louis, MO). An *mirVana*™ miRNA isolation kit was purchased from Ambion (Austin, TX). Antarctic phosphatase was purchased from New England Biolabs (Ipswich, MA). An RNeasy MiniElute Cleanup Kit was purchased from Qiagen (Valencia, CA). PCR primers were purchased from IDT (Coralville, IA). CyDye reactive dye was purchased from GE healthcare (Piscataway, NJ). Protease inhibitor cocktail and phosphatase inhibitor cocktail were purchased from Roche (Indianapolis, IN). DC protein assay and chromogenic peroxidase substrates were purchased from Bio-Rad (Hercules,

CA). Total PLCG1 rabbit polyclonal antibodies and anti-rabbit HRP-linked IgG were purchased from Cell Signaling (Beverly, MA). An MTT cell proliferation assay kit was purchased from ATCC (Manassas, VA). Oligonucleotide adaptor, hybridization station, and miRNA washing buffer were obtained from LC Sciences (Houston, TX).

2.4.2 Cell culture

Human prostate cancer cell line PC-3 was obtained from the American Type Culture Collection (ATCC) and was maintained in RPMI 1640 medium (GIBCO) supplemented with 10% fetal bovine serum (FBS, Sigma) and 1% penicillin/streptomycin at 37ºC with 5% CO_2.

2.4.3 Expression of the hybrid enzyme in PC-3 cells

PC-3 cells were cultured to ~80% confluence and transfected with COX-2-10aa-mPGES-1 plasmid cDNA (PC-3/PGE2) or transfected with pcDNA 3.1 vector alone (control PC-3) using the Lipofectamine 2000 method by following

manufacturer's instructions (Invitrogen). To enable stable expression, the transfected cells were grown with medium containing 1% geneticin (G418). Constant expression of the engineered enzyme in PC-3 cells was confirmed by western blot (Figure 2.1). The endogenous level of PGE2 in PC-3 cells was determined using HPLC method in Dr. Ke-he Ruan's lab.

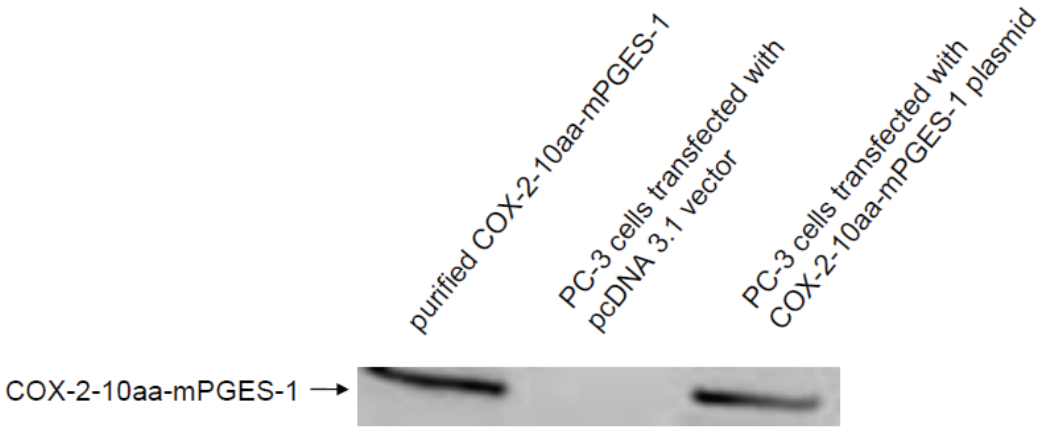

Figure 2.1: Western blots validation of hybrid enzyme COX-2-10aa-mPGES-1 expression in PC-3 cells.

Stable expression of COX-2-10aa-mPGES-1 in PC-3 cells after plasmid cDNA transfection was verified by western blots. Lane 1 was purified COX-2-10aa-mPGES-1 enzyme. Lane 2 was control PC-3 cells transfected with pcDNA 3.1 vector (control PC-3). Lane 3 was PC-3 cells transfected with COX-2-10aa-mPGES-1 plasmid and cultured in media containing 1% geneticin (G418). Experiments were repeated 3 times.

2.4.4 Total RNA extraction

Total RNA from PC-3/PGE2 and control PC-3 cells was extracted and purified with the *mirVana*™ miRNA isolation kit (Ambion) which enabled isolation of both miRNA and mRNA from the same sample. RNA concentration was determined by a NanoDrop ND-1000 spectrophotometer (Nano Drop) and RNA integrity was evaluated by an Agilent 2100 Bioanalyzer (Agilent Technologies).

2.4.5 miRNA expression profiling

Total RNA (~0.5 µg) was 3' dephosphorylated by Antarctic phosphatase to provide 3'-OH for ligation (New England Biolabs) and purified by RNeasy MiniElute Cleanup Kit (Qiagen). First, a specific oligonucleotide adaptor (LC Sciences) was ligated to the 3' of RNA for subsequent fluorescent dendrimer-dye conjugation. Then tagged RNA samples were hybridized on a µParaflo

microfluidic chip at 40 °C for 16 hours using a micro-circulation hybridization station (LC Sciences). Finally, Alexa Fluor® 3 dye conjugated with dentrimer (Invitrogen) was circulated to the sample for staining at 34 °C for 2 hours. The miRNA array was washed with washing buffer (LC Sciences) at 40°C for 20 min. Array images were acquired on a GenePix 4400B laser scanner (Molecular Device) in the 532 nm channel. For both control PC-3 cells and PC-3/PGE2 cells, miRNA microarray profiling were carried out on three biological replicates.

2.4.6 miRNA data analysis

Images were first digitalized with Array-Pro Analyzer (MediaCybernetics) to obtain signal mean and standard deviation of each probe spot on the array surface. Microarray data were further processed by background subtraction and LOWESS (Locally-weighted Regression) normalization so that biological variations between samples were identified. Differentially expressed (DE) miRNAs of PC-3/PGE2 cells versus control PC-3 cells were determined by t-test with p-value < 0.05 and fold change (FC) > 2. Heatmap and clustering of DE

miRNAs based on euclidean distance were generated by MeV software (The Institute for Genome Research).

2.4.7 mRNA probe design and probe selection

Candidate mRNAs were obtained from 4532 cancer-related genes collected from various databases. They were further classified by gene ontology (GO) enrichment analysis to explore their biological functions (http://www.geneontology.org/) (32). Genes from 11 major GO categories, such as cytokine, inflammation and receptor were selected for probe design and their corresponding mRNA sequences were obtained from NCBI (http://www.ncbi.nlm.nih.gov/). An in-house developed software probe design pipeline was employed to optimize probe performance parameters, including: probe length, melting temperature, CG percentage, and sequence complexity (lower homologous sequence content). The pipeline also refined the sequence in the complementary region of the target mRNA to ensure both the sensitivity and specificity of the probes. Final microarray layout consisted of probes for 1001 unique experimental sequences representing a comprehensive repertoire of

pivotal pathway genes and 125 house-keeping genes. Each specific sequence was represented 3 times on the array to ensure even hybridization and to monitor quality of microarray synthesis.

2.4.8 mRNA expression profiling

Total RNA from PC-3 cells and PC-3/PGE2 cells were isolated and purified. Both cells were processed in biological triplicate. Then RNA was *in vitro* transcribed and amplified into aminoallyl-labeled antisense RNA (aa-aRNA) using SuperScript Indirect RNA Amplification System (Invitrogen). The aa-aRNA was coupled to CyDye (Cy3/Cy5, GE healthcare) reactive dye for labeling prior to hybridization. CyDye-aRNA was hybridized to customized mRNA microarray when circulating at 40 °C for 16 hours within a hybridization station (LC Sciences). Cy3 samples were pooled with Cy5 samples before hybridizing to the same array. Array was scanned with a GenePix 4400B laser scanner (Molecular Device) in 532nm (Cy3) channel and 635nm (Cy5) channel respectively.

2.4.9 mRNA data analysis

Images were first digitalized with Array-Pro Analyzer (MediaCybernetics) to obtain signal mean and standard deviation of each probe spot on the array surface. mRNA expression data processing involves background correction and normalized to house-keeping genes. There were totally 25 house-keeping genes on the array and each of them had 5 probes to detect different positions of their transcripts. mRNAs with low expression level which is close to background were disqualified from further analysis. DE mRNAs were obtained by performing Student's t-test between PC-3/PGE2 cells and control PC-3 cells with a *p*-value < 0.10 and FC > 1.20 or < 0.80.

2.4.10 qRT-PCR

DE miRNAs and mRNAs determined from microarray profiling were validated by qRT-PCR using NCode^{TM} EXPRESS SYBR® GreenER^{TM} miRNA kit (Invitrogen)

on an ABI 7900HT instrument (Applied Biosystems) following manufacturers' protocols. Sequences of all the primers employed in this study were provided in Table 2.1. The ΔΔCt method was applied to calculate FCs of the surveyed miRNAs and mRNAs. The relative FCs were plotted and error bar indicated standard error of mean (SEM) from three biological replicates. Significance of differences between PC-3 and PC-3/PGE2 cells was calculated by two-tailed Student's t-test.

Table 2.1: Primers used in qRT-PCR reactions

miRNA	Primer (5' to 3')
hsa-miR-17	CAAAGTGCTTACAGTGCAGG
hsa-miR-21	TAGCTTATCAGACTGATGTTGA
hsa-miR-26a	GATTTCAAGTAATCCAGGATAGGCT
hsa-miR-26b	TTCAAGTAATTCAGGATAG
hsa-miR-146a	TGAGAACTGAATTCCATGGGTT
hsa-miR-148	GCTCAGTGCACTACAGAACTTTGT
hsa-miR-193a	GCGGGCGAGATGAAAAA
hsa-miR-200a	CGTAACACTGTCTGGTAACGATGT
hsa-miR-200b	GGTAATACTGCCTGGTAATGATGA
hsa-miR-375	CGGCTCGCGTGAAAAA
U6	CGCAAGGATGACACGCAAATTCGT
RNU48	AGTGATGATGACCCCAGGTAACTC

mRNA	Forward Primer (5' to 3')	Reverse Primer (5' to 3')
ABL2	AAAGCTACGAGTCCTTGGTTACA	GCCCATTCTTAGAGCGAACTTCA
CBL	TAGGCGAAACCTAACCAAACTG	AGAGTCCACTTGGAAAGATTCCT
CRK	GGAGACATCTTGAGAATCCGGG	GCATTCCACCACTGCTCTTC
CRKL	CTGTCGGTGTCCGAGAACTC	TGGTCCCCGATCTTAAAACGG
JAK1	AGCTCTGGTATGCTCCAAATCG	GGACATCTTGTCATCAACGGTG
MEF2C	CTGGTGTAACACATCGACCTC	GATTGCCATACCCGTTCCCT
MKNK2	CCAGCCGAACTTCAGGGTTT	GGTTCTGCCCCTTGAACGAA
VEGFA	TTATGCGGATCAAACCTCACC	GAAGCTCATCTCTCCTATGTGC
ZEB1	GTGACGCAGTCTGGGTGTAA	GTCGCCCATTCACAGGTATC
PLCG1	GTGTCCCTTCCTGAGTTCCA	GGAGGAAGCTGAGCATGAAC
DAG1	TCGAGTGACCATTCCAACAGA	CCTGCCGCTGATACCTTGA
MAP2K1	CTGCATGAGTGCAACTCTCC	GCTGTAGAACGCACCATAGAAG
MAP3K3	ACCGGATGCCTGGATATGAGA	TGAGTGACCTGTGTCTTTGTTCT
MAP4K4	GAAATGGCACCTATGGACAAGT	GCCAACTGACCCGTTTTAACA
PIK3C2A	AAATGGGACCAGTAGTTTGCC	GGGTTTGTGCGGTGATTGGTA
GAPDH	AATCCCATCACCATCTTCCA	CAGAGGGGGCAGAGATGAT
β-actin	TGGGACGACATGGAGAAAAT	CAGAGGCGTACAGGGATAGC

2.4.11 miRNA target prediction

Putative miRNA target genes of the DE miRNAs were analyzed using TargetScan Human 6.2 (http://www.targetscan.org) (33). TargetScan predicts the target genes of individual miRNA by searching the 3'-UTR of the mRNAs and determining whether they have the conserved match with the "seed" (2-7 nucleotides from 5') of miRNA in 5 genomes (human, mouse, rat, dog, and chicken). It also emphasizes the presence of either a conserved anchoring A, which is an A nucleotide downstream of the seed match on 3'-UTR of mRNA or a m8-t8 match, which is an A: U or G: C match between the eighth nucleotide from 5’ of the miRNA and its mRNA target.

2.4.12 Pathway analysis of DE miRNAs

To elucidate the enriched biological pathways in-depth and further unravel the global function of a large number of genes, either DE mRNAs or predicted target

genes of DE miRNAs identified from the study were submitted to DAVID bioinformatics resources (http://david.abcc.ncifcrf.gov) (34), a freely accessible biological database and integrative analytic tool. First, the gene list was uploaded and identifier type was selected coordinately. For instance, in our case, we uploaded gene list with identifiers as "official gene symbol". Then, appropriate species where the gene list originated was indicated. Eventually, the gene list was condensed into gene functional groups and incorporated into KEGG signaling pathways (http://www.genome.jp/kegg) (35-37). The significance of each functional group or pathway was evaluated by Fisher's exact test and represented by *p*-value.

2.4.13 Western blots

PC-3/PGE2 cells and control PC-3 cells were harvested and lysed in lysis buffer (20 mM Tris pH 6.8, 150 mM NaCl, 1% Triton X-100, 5% Glycerol, 2.5 mM sodium orthovanadate, 1x protease inhibitor cocktail (Roche) and 1x phosphatase inhibitor cocktail (Roche)) for 1 hour on ice. Cell lysates were collected by centrifuging at 13,000g for 20 min at 4 °C. Protein concentration was

estimated by DC protein assay (Bio-Rad). Approximate 25 µg of whole protein lysates were loaded into a 10% SDS-polyacrylamide gel and separated by electrophoresis at 110 V for 110 min. Protein were then transferred onto a PVDF membrane at 90 V for 90 min on ice. After transfer, membranes were block with 5% nonfat dry milk in 1x TBST (50 mM Tris pH 7.5, 150 mM NaCl, 0.1% Tween-20) at room temperature for 1 hour. Proteins to be examined were probed by corresponding specific primary antibodies in 1x TBST with 5% dry milk overnight at 4 °C. After washing, the blots were incubated with appropriate secondary antibodies which are peroxidase conjugated for 1 hour at room temperature in TBST with 5% dry milk. Immunoreactive proteins recognized by particular primary antibodies were visualized using chromogenic peroxidase substrates (Bio-Rad).

2.4.14 Cell proliferation assay

Both PC-3/PGE2 cells and control PC-3 cells were seeded at approximate 5,000 cells per well with total volume of 100 µl per well in 96-well flat bottom culture plates and allowed to grow over night at 37°C. Cell metabolism, which can

indicate proliferation, was determined every day from day 1 to day 6 after cell attachment by MTT cell proliferation assay kit (ATCC). Briefly, on each experimental day, all the wells were replaced with 100 µl of fresh culture medium and 10 µl of 3-(4, 5-dimethylthiazol-2-yl)-2, 5-diphenyl tetrazolium bromide, MTT, was added for a further four-hour incubation period at 37°C, during which time the metabolically active cells converted yellow tetrazolium salt MTT to purple precipitate. Once the purple crystals were clearly visible inside cells, 100 µl/ well of detergent was added and the plate was kept in dark at room temperature for over night reaction. Absorbance of colorimetric signal from each well was measured at 570 nm using a microtiter plate reader on the following day. The proliferation rate of PC-3/PGE2 cells was compared with that of control PC-3 cells after subtracting the intensity from no-cell blank control wells. All assays were performed in triplicate and diagram represented average absorbance and standard error of mean from them.

2.5 Results

2.5.1 Excessive endogenous PGE2 elicited differential expression of miRNAs

The endogenous level of PGE2 in PC-3 cells was determined using HPLC method in Dr. Ke-he Ruan's lab. They showed that majority of AA was specifically converted into PGE2 in PC-3/PGE2 cells. To explore the alterations in miRNAs expression when the PGE2 level was induced, the miRNA profile of PC-3/PGE2 cells was compared with that of control PC-3 cells. In total, 1,212 unique human mature miRNAs from miRBase version 16 were examined by microarray assays (27). We found that 65 miRNAs were downregulated and 34 were upregulated with $p < 0.1$ after T-test in response to over-production of PGE2 (Table 2.2 and Table 2.3). Moreover, after refining the criteria of significant DE miRNAs to $p < 0.05$ with 2-fold cut off, 30 miRNAs were down and 18 were upregulated, which were used for subsequent analysis. Alternations in the expression of DE miRNAs and their distances (similarity) were displayed by conducting a Heatmap analysis with hierarchical clustering (Figure 2.2).

We surveyed 17 DE miRNAs along with RNU48 and U6 as endogenous controls by performing miRNA qRT-PCR on PC-3/PGE2 cells and control PC-3 cells to further validate their expression level. Nine out of 17 where significantly changed when confirmed using qRT-PCR (Figure 2.3) and supported the reproducibility and reliability of data obtained.

Table 2.2: miRNAs downregulated in PC-3/PGE2 cells

Index	miRNA ID	Log2(FC)	*p*-value
1	hsa-miR-433	-18.19	1.59E-02
2	hsa-miR-455-5p	-14.96	2.64E-02
3	hsa-miR-585	-14.81	8.01E-03
4	hsa-miR-659	-8.35	4.78E-02
5	hsa-miR-664*	-6.37	7.85E-02
6	hsa-miR-375	-4.82	1.79E-02
7	hsa-miR-101	-3.57	4.73E-03
8	hsa-miR-4324	-3.13	1.25E-03
9	hsa-miR-1287	-2.86	1.32E-02
10	hsa-miR-342-3p	-2.74	6.83E-03
11	hsa-miR-4252	-2.62	5.57E-02
12	hsa-miR-454	-2.62	3.43E-02
13	hsa-miR-200a	-2.58	5.58E-03
14	hsa-miR-223	-2.34	4.81E-02
15	hsa-miR-4267	-2.33	2.23E-02
16	hsa-miR-181c	-2.24	8.05E-02
17	hsa-miR-200b	-2.08	2.99E-03
18	hsa-miR-3647-3p	-2.08	7.54E-03
19	hsa-miR-26b	-2.02	9.81E-04
20	hsa-miR-148b	-2.02	1.39E-02
21	hsa-miR-21	-1.88	8.89E-03
22	hsa-miR-652	-1.86	4.91E-03
23	hsa-miR-195	-1.77	7.87E-02
24	hsa-miR-3651	-1.61	6.75E-02
25	hsa-miR-4258	-1.57	4.59E-02
26	hsa-miR-146a	-1.51	1.20E-04
27	hsa-miR-29b-2*	-1.48	9.02E-02
28	hsa-miR-3661	-1.45	8.47E-02
29	hsa-miR-1973	-1.44	2.01E-02
30	hsa-miR-3647-5p	-1.43	5.07E-03
31	hsa-miR-4312	-1.38	8.58E-02
32	hsa-miR-425*	-1.35	9.20E-02
33	hsa-miR-320e	-1.31	2.66E-02
34	hsa-miR-1180	-1.24	3.59E-02
35	hsa-miR-181a	-1.21	4.09E-02
36	hsa-miR-424*	-1.20	7.04E-02
37	hsa-miR-4279	-1.17	5.46E-02
38	hsa-miR-1246	-1.12	3.05E-03
39	hsa-miR-193a-3p	-1.11	9.21E-03

Table 2.2 (cont.)

Index	miRNA ID	Log2(FC)	*p*-value
40	hsa-miR-3609	-1.11	1.01E-03
41	hsa-miR-3676	-1.02	3.99E-02
42	hsa-miR-572	-1.01	6.70E-02
43	hsa-miR-502-3p	-0.99	9.25E-02
44	hsa-miR-140-3p	-0.92	7.29E-03
45	hsa-miR-518d-3p	-0.91	6.80E-02
46	hsa-miR-484	-0.84	2.85E-02
47	hsa-miR-30b	-0.82	5.12E-02
48	hsa-miR-362-5p	-0.81	1.48E-02
49	hsa-miR-320b	-0.81	6.08E-02
50	hsa-miR-320d	-0.75	8.59E-02
51	hsa-miR-320c	-0.73	6.14E-02
52	hsa-miR-320a	-0.69	6.02E-02
53	hsa-miR-551b	-0.67	6.93E-02
54	hsa-miR-532-5p	-0.66	3.26E-02
55	hsa-miR-568	-0.64	9.36E-03
56	hsa-miR-26a	-0.63	4.91E-03
57	hsa-let-7g	-0.62	7.27E-02
58	hsa-miR-636	-0.61	6.34E-03
59	hsa-miR-500b	-0.6	9.01E-02
60	hsa-let-7b	-0.56	5.64E-02
61	hsa-miR-30d	-0.52	7.85E-02
62	hsa-miR-210	-0.35	1.14E-03
63	hsa-let-7f	-0.31	3.44E-02
64	hsa-let-7a	-0.3	2.48E-02
65	hsa-miR-100	-0.29	2.82E-02

Table 2.3: miRNAs upregulated in PC-3/PGE2 cells

Index	miRNA ID	Log2(FC)	*p*-value
1	hsa-miR-1261	6.92	7.45E-02
2	hsa-miR-590-5p	5.38	9.17E-02
3	hsa-miR-498	5.33	1.83E-02
4	hsa-miR-548m	4.11	3.86E-02
5	hsa-miR-548h	3.60	1.29E-02
6	hsa-miR-1469	2.99	4.13E-05
7	hsa-miR-889	2.86	6.03E-02
8	hsa-miR-762	2.61	3.35E-05
9	hsa-miR-3196	1.81	2.91E-03
10	hsa-miR-3656	1.80	3.72E-03
11	hsa-miR-1915	1.80	1.51E-02
12	hsa-miR-4281	1.77	4.02E-02
13	hsa-miR-3178	1.67	3.28E-03
14	hsa-miR-638	1.62	1.77E-02
15	hsa-miR-3195	1.58	1.63E-03
16	hsa-miR-3665	1.51	8.69E-04
17	hsa-miR-663	1.46	2.53E-02
18	hsa-miR-18a	1.34	8.34E-02
19	hsa-miR-3190	1.20	1.36E-02
20	hsa-miR-301a	1.17	3.99E-04
21	hsa-miR-3141	1.13	5.26E-03
22	hsa-miR-1280	1.01	1.13E-02
23	hsa-miR-3679-5p	0.94	8.07E-02
24	hsa-miR-23a	0.89	1.10E-02
25	hsa-miR-17	0.88	1.06E-02
26	hsa-miR-149*	0.86	5.91E-02
27	hsa-miR-3149	0.81	6.45E-03
28	hsa-miR-20a	0.76	1.25E-02
29	hsa-miR-574-5p	0.75	1.43E-02
30	hsa-miR-425	0.70	1.32E-02
31	hsa-miR-601	0.54	3.50E-02
32	hsa-miR-93	0.51	1.62E-02
33	hsa-miR-23b	0.44	8.83E-02
34	hsa-miR-361-5p	0.29	4.77E-02

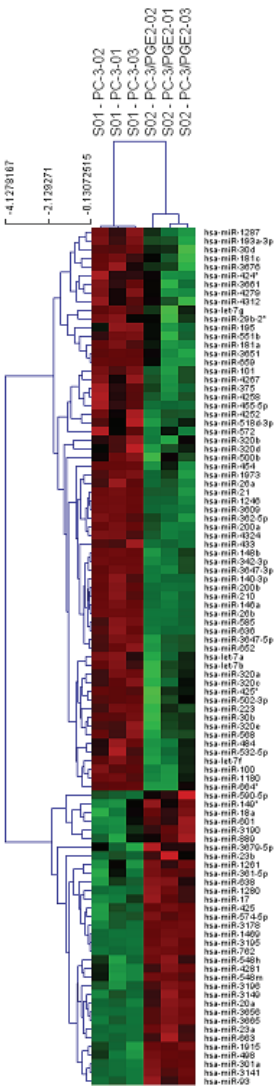

Figure 2.2: Heatmap and hierarchical clustering of DE miRNAs in response to PGE2

Each row represented a miRNA and each column a sample. Dendrograms at the top and on the left side indicated the euclidean distance among samples or miRNAs. Red and Green color denoted Z-value ranging from -1.5 to 0 to +1.5, although values at each maximal color may exceed that amount. Red represented high expression level which is above the mean and green low expression. Detailed expression and FCs of miRNAs were shown in Table 2.2 and Table 2.3.

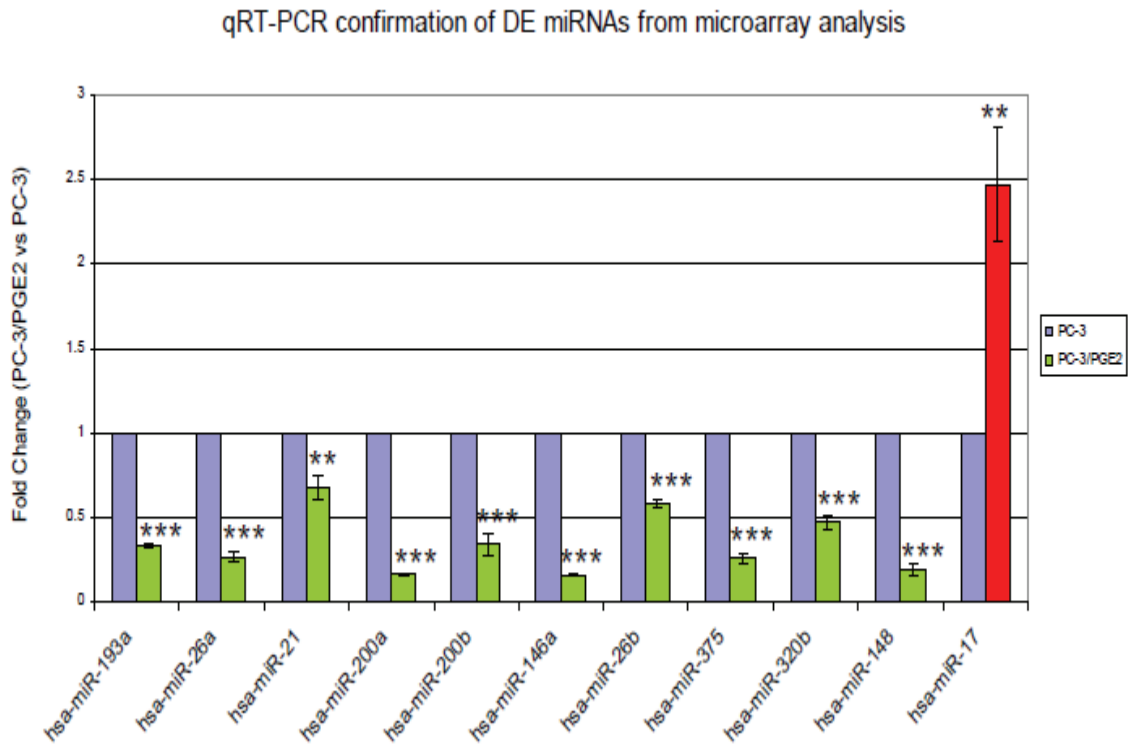

Figure 2.3: qRT-PCR validation of selected DE miRNAs identified from miRNA microarray

Quantitative of miRNA expression in PC-3/PGE2 cells and in control PC-3 cells was obtained by qRT-PCR. U6 and RNU48 small RNAs were applied as endogenous house-keeping genes. The height of columns indicated FCs of miRNA expression for PC-3/PGE2 cells versus control PC-3 cells (control FCs were set to one). Error bars depicted SEM of three biological replicates. Significance of differences between PC-3 cells (control) and PC-3/PGE2 cells was calculated by two-tailed Student's t-test and are represented by *p*-value. *** represented a *p*-value < 0.001, ** represented a *p*-value < 0.01, * represented a *p*-value < 0.05, no asterisk represented no significant differences (*p*-value > 0.05).

2.5.2 Target prediction and pathway enrichment analysis of DE miRNAs

miRNAs exert their biological function mainly by altering expression level of their target genes. To elucidate the crucial role of a specific DE miRNA, we initially predicted its potential target genes with the aid of TargetScan Human 6.2 (33), and then conducted pathway enrichment analysis on all the target genes by applying DAVID bioinformatics resources (34). The number of target genes that had been predicted for each DE miRNA by TargetScan and the top most enriched KEGG pathways for the putative target genes based on DAVID pathway enrichment analysis were summarized in Table 2.4.

Essential pathways associated with the downregulated miRNAs were pathways in cancer (five out of 30 miRNAs), the MAPK pathway (five out of 30 miRNAs), and Neurotrophin signaling pathway (three out of 30 miRNAs). Meanwhile, the notable pathway with respect to upregulated miRNAs was pathway in cancer (two out of 18 miRNAs) (Table 2.4). Intriguingly, downregulated miRNAs, (*e.g.,*

miR-101, -146, -148, -181, -193, -200, -21, -26, and -375) had been studied by different groups and reported in previous publications; while upregulated miRNAs (*e.g.*, miR-1280, -301, -3141, -3665, -498, and -548) lacked target and corresponding pathway information.

Table 2.4: Target prediction and pathway enrichment analysis of significant DE miRNAs in PC-3/PGE2

DE miRNA ID	No. of conserved targets	No. of targets found in KEGG pathways	Top1 enriched KEGG pathway	No. of targets in Top1 enriched pathway	*p*-value for Top1 pathway
miR-101	803	213	Pathways in cancer	32	1.10E-05
miR-1180	13	7	Pancreatic cancer	2	8.20E-02
miR-1246	178	42	Neuroactive ligand-receptor interaction	7	1.60E-02
miR-1287	162	29	MAPK signaling pathway	8	4.60E-04
miR-146a	224	55	Pathways in cancer	10	7.00E-03
miR-148b	698	198	Focal adhesion	20	2.50E-04
miR-181a	1194	310	Neurotrophin signaling pathway	21	4.70E-05
miR-193a-3p	221	56	Pathways in cancer	13	1.50E-04
miR-1973	25	5	N/A		
miR-200a	744	185	Pathways in cancer	26	2.70E-04
miR-200b	1057	290	Neurotrophin signaling pathway	32	7.00E-13
miR-21	307	89	MAPK signaling pathway	17	1.00E-05
miR-223	311	84	Prostate cancer	7	3.10E-03
miR-26b	885	219	Wnt signaling pathway	18	2.20E-04
miR-320e	296	75	Hypertrophic cardiomyopathy (HCM)	7	1.40E-03
miR-342-3p	282	79	Long-term potentiation	5	2.00E-02
miR-3609	865	238	Pathways in cancer	38	2.80E-07
miR-3647-3p	927	248	Ubiquitin mediated proteolysis	19	9.40E-05
miR-3647-5p	206	61	Calcium signaling pathway	7	1.70E-02
miR-3676	13	5	N/A		
miR-375	229	62	Maturity onset diabetes of the young	3	3.60E-02
miR-4258	28	10	Non-small cell lung cancer	2	9.20E-02
miR-4267	442	114	MAPK signaling pathway	13	1.50E-02
miR-4324	923	236	MAPK signaling pathway	24	2.60E-03
miR-433	317	91	Oocyte meiosis	10	1.20E-04
miR-454	899	248	Endocytosis	27	6.00E-07
miR-455-5p	199	49	Adherens junction	5	5.70E-03
miR-585	5	1	N/A		
miR-652	8	2	N/A		
miR-659	697	175	MAPK signaling pathway	21	7.00E-04
miR-1280	*88*	*29*	*Neurotrophin signaling pathway*	*4*	*3.00E-02*
miR-1469	*2*	*2*	*N/A*		
miR-1915	*354*	*87*	*Pathways in cancer*	*12*	*2.10E-02*
miR-301a	*899*	*248*	*Endocytosis*	*27*	*6.00E-07*
miR-3141	*11*	*4*	*Endometrial cancer*	*2*	*3.00E-02*
miR-3178	*10*	*2*	*N/A*		
miR-3190	*225*	*56*	*Lysosome*	*6*	*8.20E-03*
miR-3195	*5*	*1*	*N/A*		
miR-3196	*50*	*12*	*Small cell lung cancer*	*3*	*1.30E-02*
miR-3656	*21*	*5*	*Cell adhesion molecules (CAMs)*	*2*	*1.00E-01*
miR-3665	*292*	*79*	*Axon guidance*	*8*	*3.40E-03*
miR-4281	*203*	*62*	*Adherens junction*	*6*	*2.10E-03*
miR-498	*547*	*136*	*Wnt signaling pathway*	*12*	*2.10E-03*
miR-548h	*659*	*162*	*Pathways in cancer*	*22*	*1.40E-03*

Note: Italic: upregulated miRNAs in PC-3/PGE2 cells compared to control PC-3 cells

2.5.3 Increased biosynthesis of PGE2 altered gene expression at mRNA level

To assess the impact of enhanced intracellular PGE2 level in the context of gene expression, we systematically profiled mRNA transcripts from PC-3 and PC-3/PGE2 cells using mRNA expression microarrays. The probe content of mRNA microarray was determined by analysis and clustering of 4,532 cancer-related genes according to gene ontology classification (32). Probes for 1,001 genes which belonged to cytokine, inflammation, and receptor were included in the array. After t-test, expression of 124 mRNAs was upregulated and 106 downregulated upon increase of PGE2 (p-value < 0.10 and FC > 1.20 or < 0.80) (Table 2.5 and Table 2.6). 28 DE mRNAs were validated by qRT-PCR (Figure 2.4) and all of them showed consistent expression with microarray results.

Table 2.5: mRNAs upregulated in PC-3/PGE2 cells

Index	Official gene symbol	Accession no.	FC	*p*-value
1	C13ORF15	NM_014059	4.06	5.75E-14
2	NCF2	NM_000433	3.54	4.48E-13
3	CXCL1	NM_001511	3.32	2.63E-02
4	SGK1	NM_005627	3.19	6.46E-02
5	AKAP2	NM_007203	3.17	0.00E+00
6	SPHK1	NM_021972	3.14	0.00E+00
7	CDC6	NM_001254	3.04	2.56E-04
8	RPSA	NM_002295	2.73	8.88E-16
9	DRD1	NM_000794	2.7	8.25E-08
10	TK1	NM_003258	2.59	4.82E-07
11	EPHB6	NM_004445	2.48	8.67E-06
12	CXCL6	NM_002993	2.41	9.30E-04
13	PIM2	NM_006875	2.39	2.65E-06
14	PLAU	NM_002658	2.31	0.00E+00
15	TNFSF15	NM_005118	2.29	1.44E-02
16	EIF2C2	NM_012154	2.24	0.00E+00
17	DDIT3	NM_004083	2.23	0.00E+00
18	FGFR4	NM_002011	2.2	7.64E-02
19	CCNE1	NM_001238	2.12	3.85E-03
20	PIK3CD	NM_005026	2.05	1.23E-11
21	CDKN1C	NM_000076	1.93	0.00E+00
22	FER	NM_005246	1.9	1.39E-05
23	TYRO3	NM_006293	1.89	3.47E-04
24	EPHB2	NM_004442	1.89	7.69E-02
25	CDC20	NM_001255	1.86	7.82E-08
26	CXCR4	NM_003467	1.8	4.35E-06
27	TMED7	NM_021649	1.75	4.31E-05
28	CD70	NM_001252	1.74	1.13E-03
29	EIF2C3	NM_024852	1.72	5.01E-02
30	IGF2R	NM_000876	1.71	1.21E-10
31	CDKN1A	NM_000389	1.69	1.26E-03
32	MKNK2	NM_017572	1.67	0.00E+00
33	MC1R	NM_006086	1.66	6.50E-04
34	HK1	NM_000188	1.66	1.38E-06
35	NFYA	NM_002505	1.64	2.90E-03

Table 2.5 (cont.)

Index	Official gene symbol	Accession no.	FC	*p*-value
36	CCL26	NM_006072	1.63	7.91E-02
37	CSNK1D	NM_001893	1.63	7.86E-10
38	MLH1	NM_000249	1.63	0.00E+00
39	RIPK2	NM_003821	1.62	6.00E-15
40	FUT8	NM_178157	1.61	0.00E+00
41	IFNAR2	NM_000874	1.6	1.59E-03
42	RBM3	NM_006743	1.6	6.34E-12
43	PARD3	NM_019619	1.58	4.14E-03
44	UBE2C	NM_181803	1.57	0.00E+00
45	MAP3K3	NM_002401	1.56	1.20E-04
46	BMP2K	NM_198892	1.56	1.60E-08
47	GDF15	NM_004864	1.54	6.78E-13
48	PTK7	NM_002821	1.53	6.28E-04
49	GSK3B	NM_002093	1.53	8.13E-02
50	CDC42BPA	NM_003607	1.53	4.18E-09
51	PVR	NM_006505	1.53	1.04E-07
52	PLK2	NM_006622	1.52	5.61E-04
53	MVD	NM_002461	1.51	9.89E-03
54	CSNK1E	NM_001894	1.5	5.10E-14
55	SOCS2	NM_003877	1.5	3.65E-02
56	PRKCZ	NM_002744	1.48	1.09E-09
57	CDC25B	NM_004358	1.48	3.37E-07
58	LMNA	NM_005572	1.48	2.78E-08
59	GPI	NM_000175	1.47	4.81E-14
60	FHL1	NM_001449	1.47	0.00E+00
61	BMP8B	NM_001720	1.47	8.32E-07
62	LOC344593	NM_002834	1.46	7.46E-07
63	SREBF2	NM_004599	1.46	2.33E-04
64	ACVR1	NM_001105	1.45	5.47E-07
65	PDK1	NM_002610	1.44	9.03E-02
66	ABL2	NM_005158	1.42	1.06E-03
67	HSPH1	NM_006644	1.42	1.83E-08
68	PIK3C2A	NM_002645	1.42	1.83E-04
69	DLG4	NM_001365	1.42	8.20E-02
70	PAK1	NM_002576	1.42	3.19E-02

Table 2.5 (cont.)

Index	Official gene symbol	Accession no.	FC	*p*-value
71	MAP4K4	NM_004834	1.41	0.00E+00
72	DSP	NM_004415	1.4	7.93E-05
73	TNFSF14	NM_003807	1.4	5.18E-02
74	ARRB2	NM_004313	1.4	5.40E-04
73	TNFSF14	NM_003807	1.4	5.18E-02
74	ARRB2	NM_004313	1.4	5.40E-04
75	GNB2	NM_005273	1.39	7.66E-03
76	PPM1D	NM_003620	1.38	6.25E-02
77	SH2B2	NM_020979	1.38	3.02E-03
78	PTTG2	NM_004219	1.37	1.27E-03
79	CDK10	NM_00109853	1.37	1.43E-06
80	E2F3	NM_001949	1.37	6.29E-03
81	CHST2	NM_004267	1.37	3.95E-02
82	IL18	NM_001562	1.36	8.87E-03
83	ADAM17	NM_003183	1.36	3.75E-04
84	GNAS	NM_080425	1.36	4.25E-13
85	SLK	NM_014720	1.34	2.52E-02
86	ADAM19	NM_033274	1.34	1.35E-03
87	PLCG1	NM_002660	1.34	6.34E-02
88	PPP1CA	NM_002708	1.33	3.78E-03
89	PRKAR1A	NM_002734	1.32	3.08E-06
90	CDKN2A	NM_000077	1.32	3.64E-05
91	LOC407835	NM_030662	1.32	2.80E-02
92	CETN2	NM_004344	1.31	1.39E-04
93	INPPL1	NM_001567	1.31	7.45E-04
94	CDK4	NM_000075	1.31	1.34E-03
95	PIK3CG	NM_002649	1.31	1.44E-03
96	MEF2C	NM_002397	1.31	5.85E-02
97	JAK1	NM_002227	1.3	2.98E-06
98	PFKP	NM_002627	1.29	1.50E-02
99	PIM1	NM_002648	1.29	6.01E-03
100	RGS19	NM_005873	1.29	2.72E-03
101	PGK1	NM_000291	1.29	6.83E-03
102	CSNK2A1	NM_001895	1.29	7.37E-03
103	ABI2	NM_005759	1.28	3.46E-02
104	SOCS6	NM_004232	1.28	9.40E-03
105	BCR	NM_004327	1.28	9.90E-02

Table 2.5 (cont.)

Index	Official gene symbol	Accession no.	FC	*p*-value
106	BAZ1B	NM_032408	1.27	1.33E-02
107	CRKL	NM_005207	1.26	1.71E-04
108	TCF3	NM_003200	1.26	3.16E-02
109	TSPYL2	NM_022117	1.26	4.81E-05
110	MAP2K1	NM_002755	1.25	5.39E-03
111	MADD	NM_003682	1.25	7.52E-02
112	CRK	NM_016823	1.25	6.12E-04
113	ILK	NM_004517	1.25	1.11E-04
114	PRKACA	NM_002730	1.23	5.90E-03
115	CBL	NM_005188	1.23	5.11E-02
116	CDK13	NM_003718	1.23	2.02E-03
117	LOC642954	NM_005610	1.23	2.14E-02
118	CKS2	NM_001827	1.23	1.90E-03
119	DAG1	NM_004393	1.22	8.93E-02
120	SIRPA	NM_080792	1.22	2.21E-02
121	BCAR3	NM_003567	1.21	8.21E-04
122	IRAK1	NM_001569	1.21	8.93E-08
123	PTPN11	NM_002834	1.2	2.41E-03
124	CXCR5	NM_001716	1.2	2.28E-02

Table 2.6: mRNAs downregulated in PC-3/PGE2 cells

Index	Official gene symbol	Accession no.	FC	*p*-value
1	TNFSF10	NM_003810	0.07	0.00E+00
2	C4A	NM_007293	0.16	4.57E-06
3	BMP3	NM_001201	0.2	2.55E-08
4	STAT1	NM_007315	0.26	1.44E-15
5	BSN	NM_003458	0.3	8.57E-02
6	IL7	NM_000880	0.32	1.80E-02
7	STAT2	NM_005419	0.36	0.00E+00
8	IL1A	NM_000575	0.36	4.39E-02
9	RGS2	NM_002923	0.41	0.00E+00
10	KDR	NM_002253	0.45	0.00E+00
11	NR2F1	NM_005654	0.45	0.00E+00
12	VEGFA	NM_003376	0.46	0.00E+00
13	KAT2B	NM_003884	0.46	0.00E+00
14	BMPR1B	NM_001203	0.48	0.00E+00
15	PIK3R3	NM_003629	0.49	6.04E-11
16	BRS3	NM_001727	0.49	2.00E-02
17	SH2D4A	NM_022071	0.5	1.57E-02
18	IL29	NM_172140	0.5	7.55E-02
19	C5	NM_001735	0.5	0.00E+00
20	NBN	NM_002485	0.51	2.16E-07
21	IFNGR1	NM_000416	0.51	2.06E-11
22	GDF11	NM_005811	0.51	2.47E-04
23	CDKN1B	NM_004064	0.52	1.11E-15
24	CSNK1A1	NM_001892	0.52	0.00E+00
25	LOC651610	NM_000051	0.53	7.66E-09
26	TNFSF4	NM_003326	0.53	2.39E-02
27	ACTA1	NM_001100	0.55	8.25E-03
28	PIK3CB	NM_006219	0.56	1.32E-03
29	LHCGR	NM_000233	0.56	3.77E-05
30	EIF2AK2	NM_002759	0.57	1.18E-05
31	NDC80	NM_006101	0.58	6.79E-04
32	MAP2K6	NM_002758	0.59	4.47E-02
33	CABC1	NM_020247	0.59	3.06E-08
34	RCBTB1	NM_018191	0.59	7.35E-03
35	DNAJC19	NM_145261	0.6	5.80E-04

Table 2.6 (cont.)

Index	Official gene symbol	Accession no.	FC	*p*-value
36	SH3BP2	NM_003023	0.62	5.69E-02
37	TFDP2	NM_006286	0.62	4.49E-02
38	CLK1	NM_004071	0.62	9.39E-07
39	SPHK2	NM_020126	0.63	1.02E-02
40	PKLR	NM_000298	0.63	6.80E-02
41	SHC4	NM_203349	0.63	6.82E-04
42	RBL2	NM_005611	0.64	1.89E-06
43	ERBB2	NM_004448	0.64	2.94E-03
44	LOC648152	NM_001184	0.64	7.93E-04
45	TNNI3	NM_000363	0.64	4.80E-05
46	ANAPC11	NM_001002244	0.65	8.64E-02
47	TJP1	NM_175610	0.66	0.00E+00
48	CSNK1G3	NM_004384	0.66	2.44E-02
49	CDK1	NM_001786	0.66	1.88E-04
50	CIT	NM_007174	0.66	3.59E-05
51	CCNG1	NM_004060	0.67	0.00E+00
52	RPS6KA6	NM_014496	0.68	5.57E-02
53	TPM1	NM_000366	0.68	9.14E-05
54	NEK6	NM_014397	0.68	9.18E-02
55	PPP1R13B	NM_015316	0.69	1.70E-02
56	NR2F2	NM_021005	0.69	4.67E-11
57	EVL	NM_016337	0.7	7.28E-02
58	PRKCH	NM_006255	0.7	1.22E-03
59	PRKACB	NM_182948	0.7	2.74E-02
60	MAPKSP1	NM_021970	0.7	7.88E-02
61	SSSCA1	NM_006396	0.71	7.96E-05
62	CCND1	NM_053056	0.71	1.03E-10
63	CDKN2B	NM_004936	0.71	1.40E-08
64	RPS6KB1	NM_003161	0.71	1.88E-04
65	STYK1	NM_018423	0.71	8.11E-02
66	PARD6B	NM_032521	0.71	4.62E-02
67	SOX4	NM_003107	0.71	2.50E-05
68	SMC4	NM_005496	0.72	8.07E-04
69	DLG3	NM_021120	0.72	1.22E-04
70	ING1	NM_005537	0.72	9.30E-04

Table 2.6 (cont.)

Index	Official gene symbol	Accession no.	FC	*p*-value
71	PIK3C2B	NM_002646	0.73	1.74E-03
72	SPDYA	NM_002709	0.73	1.01E-04
73	GNAO1	NM_020988	0.73	4.38E-02
74	PTP4A1	NM_003463	0.73	5.73E-03
75	CCNG2	NM_004354	0.73	4.97E-02
76	GNPTG	NM_032520	0.73	7.50E-06
77	NME4	NM_005009	0.74	1.21E-04
78	LY6G5B	NM_001320	0.74	1.07E-04
79	RACGAP1P	NM_013277	0.74	6.84E-02
80	EPS15	NM_001981	0.74	1.77E-02
81	PRKDC	NM_006904	0.74	4.39E-06
82	CCNB1	NM_031966	0.74	1.22E-03
83	KRT18P19	NM_000224	0.75	5.37E-05
84	ILF3	NM_004516	0.76	1.26E-07
85	MST1R	NM_002447	0.76	8.39E-03
86	ANXA11	NM_001157	0.76	1.60E-03
87	PRKCD	NM_006254	0.76	9.08E-02
88	STAT6	NM_003153	0.76	1.08E-02
89	PDK2	NM_002611	0.77	3.85E-02
90	MAP4K3	NM_003618	0.77	3.61E-05
91	AKT1	NM_005163	0.77	1.33E-03
92	CXCL5	NM_002994	0.77	4.20E-02
93	DCK	NM_000788	0.78	8.47E-04
94	CALM3	NM_006888	0.78	4.37E-03
95	TSG101	NM_006292	0.78	2.88E-03
96	HK2P1	NM_000189	0.78	6.02E-06
97	IFNAR1	NM_000629	0.78	2.72E-03
98	CDKN3	NM_005192	0.79	5.77E-04
99	RASSF1	NM_007182	0.79	1.83E-06
100	REG3G	NM_198448	0.79	5.11E-02
101	AHR	NM_001621	0.79	1.49E-04
102	PAFAH1B1	NM_000430	0.79	5.25E-04
103	HCK	NM_002110	0.79	9.05E-02
104	CTTN	NM_005231	0.8	1.50E-10
105	AREGB	NM_001657	0.8	7.18E-10
106	EPHB3	NM_004443	0.8	3.24E-03

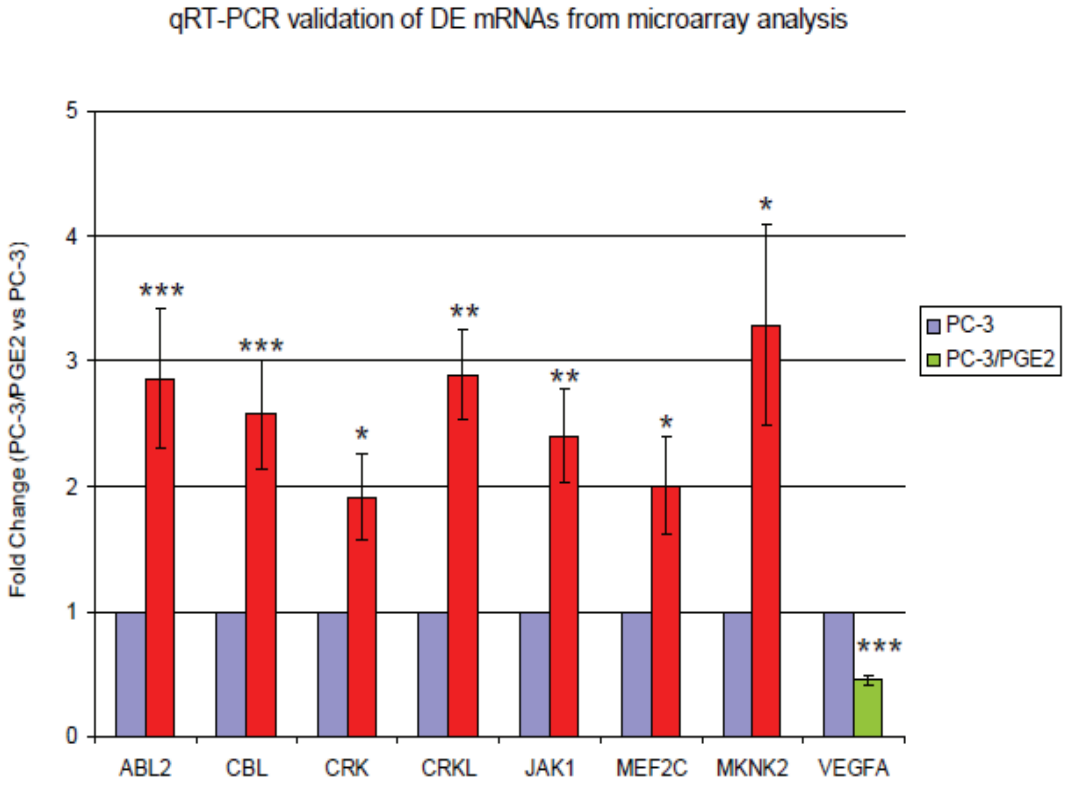

Figure 2.4: qRT-PCR validation of DE mRNAs identified from mRNA expression microarray

Relative mRNA expression in PC-3/PGE2 cells and control PC-3 cells were assessed by qRT-PCR. GAPDH and β-actin mRNAs were used as house-keeping genes. Expression of target mRNAs was normalized to GAPDH. The height of columns indicated FCs of mRNA expression between PC-3/PGE2 cells and control PC-3 cells (control FCs were set to one). Error bars were SEM of three biological replicates. Significance of differences between PC-3 cells (control) and PC-3/PGE2 cells was calculated by two-tailed Student's t-test and are represented by p-value. *** represented a p-value < 0.001, ** represented a p-value < 0.01, * represented a p-value < 0.05, no asterisk represented no significant differences (p-value > 0.05).

2.5.4 DE mRNAs were enriched in specific pathways

Furthermore, we estimated the putative affected signaling pathways by DE mRNAs using the NIH/DAVID pathway enrichment analysis tool. All the genes in KEGG signaling pathways were applied as background. The significance of enrichment was calculated by Fisher's exact test and represented by *p*-value. Based on our results, 108 among the 124 upregulated mRNAs were accompanied with KEGG pathway annotation; in contrast, 72 out of 106 downregulated mRNAs were associated with KEGG pathways (35-37). The upregulated mRNAs are mainly involved in the insulin signaling pathway, meanwhile, the downregulated mRNAs are primarily implicated in the Jak-Stat signaling pathway (Table 2.7 and Table 2.8).

Table 2.7: Pathway enrichment analysis of upregulated mRNAs in PC-3/PGE2 according to KEGG signaling pathways

(p-value < 0.01).

Enriched pathway	Gene count	p-value	Genes
Insulin signaling pathway	16	1.90E-08	PIK3CG, PRKCZ, SOCS2, MAP2K1, PIK3CD, CBL, MKNK2, HK1, LOC407835, PPP1CA, CRKL, GSK3B, PRKAR1A, SH2B2, PRKACA, CRK
Chemokine signaling pathway	17	2.54E-07	CXCL1, PIK3CG, PRKCZ, PARD3, MAP2K1, PIK3CD, CXCL6, CCL26, CRKL, ARRB2, GNB2, CXCR5, CXCR4, GSK3B, PRKACA, PAK1, CRK
Neurotrophin signaling pathway	14	3.68E-07	PIK3CG, PDK1, IRAK1, MAP2K1, PIK3CD, LOC344593, PTPN11, LOC407835, CRKL, MAP3K3, PLCG1, GSK3B, RIPK2, SH2B2, CRK
ErbB signaling pathway	12	4.68E-07	PIK3CG, LOC407835, CDKN1A, CRKL, PLCG1, MAP2K1, GSK3B, PIK3CD, CBL, PAK1, CRK, ABL2
T cell receptor signaling pathway	10	1.61E-04	PDK1, PIK3CG, LOC407835, PLCG1, MAP2K1, GSK3B, PIK3CD, CBL, PAK1, CDK4
MAPK signaling pathway	14	1.25E-03	MEF2C, FGFR4, MAP2K1, MKNK2, DDIT3, CDC25B, LOC407835, MAP4K4, CRKL, ARRB2, MAP3K3, PRKACA, PAK1, CRK

Table 2.8: Pathway enrichment analysis of downregulated mRNAs in PC-3/PGE2 according to KEGG signaling pathways

(p-value < 0.01)

Enriched pathway	Gene count	p-value	Genes
Jak-STAT signaling pathway	11	4.83E-05	STAT6, AKT1, CCND1, IL29, IL7, PIK3CB, PIK3R3, STAT1, IFNGR1, STAT2, IFNAR1
Insulin signaling pathway	10	9.25E-05	SPDYA, HK2P1, AKT1, PIK3CB, PKLR, CALM3, RPS6KB1, PRKACB, PIK3R3, SHC4
ErbB signaling pathway	8	1.84E-04	AKT1, CDKN1B, PIK3CB, ERBB2, RPS6KB1, AREGB, PIK3R3, SHC4
p53 signaling pathway	7	3.31E-04	LOC651610, CCNB1, CDK1, CCND1, LOC648152, CCNG1, CCNG2
mTOR signaling pathway	6	7.19E-04	AKT1, RPS6KA6, PIK3CB, VEGFA, RPS6KB1, PIK3R3
Chemokine signaling pathway	10	1.05E-03	AKT1, CXCL5, PIK3CB, HCK, PRKACB, PIK3R3, STAT1, PRKCD, STAT2, SHC4
VEGF signaling pathway	6	3.73E-03	AKT1, SPHK2, PIK3CB, VEGFA, PIK3R3, KDR
Neurotrophin signaling pathway	7	7.32E-03	AKT1, RPS6KA6, PIK3CB, CALM3, PIK3R3, PRKCD, SHC4

2.5.5 Integrative analysis of DE miRNA and mRNA profiles

We concurrently profiled miRNA and mRNA expression level in PC-3/PGE2 cells and compared them with the level in PC-3 control cells. We found that increased biosynthesis of PGE2 largely elicited the differential expression of both miRNAs and mRNAs. DE mRNAs were involved in major signaling pathways, whereas miRNAs may potentially interact and negative regulate mRNAs of their target genes at post-transcriptional level. To better elucidate the putative miRNA-mRNA-pathway framework altered by upregulation of PGE2, we identified the anticorrelated miRNA:mRNA pairs based on their expression profiles (Table 2.9). One single miRNA may target and regulate multiple genes and one gene may be targeted and regulated by multiple miRNAs after transcription. Our miRNA;mRNA integrative analysis approach determined putative miRNA:mRNA pairs which were altered by over-production of PGE2. miRNA target prediction was carried out *in silico*. Meanwhile, inverse correlated expression profiles between miRNA and their predicted targets provided another layer of evidence for their possible interaction. According to known pathway annotations for target mRNAs, we are

able to first link miRNAs to their predicted targets and then implicate miRNAs into pathways.

Table 2.9: Anticorrelated miRNA:mRNA pairs identified by integrative microarray profile analysis in PC-3/PGE2 cells

Downregulated miRNAs	Upregulated mRNAs
miR-101	GSK3B, SOCS2
miR-1246	GSK3B
miR-146a	ABL2, IRAK1
miR-148b	ABL2, CDC25B, PDK1
miR-181a	ABL2, MAP2K1, MAP3K3, MAP4K4, MKNK2
miR-193a-3p	MAP3K3
miR-200a	ABL2, CBL, CDC25B, MAP3K3, MAP4K4, PRKAR1A
miR-200b	CBL, CRKL, MAP4K4, PLCG1, PRKAR1A, PTPN11
miR-21	MEF2C
miR-223	MEF2C
miR-26b	ABL2, GSK3B, MEF2C, MKNK2
miR-320e	CRKL, MAP3K3
miR-3609	CRK, GSK3B, MEF2C, MKNK2
miR-3647-3p	ABL2, CBL, CRK, CXCR5, MEF2C, PTPN11
miR-4267	GSK3B, MAP3K3, MEF2C, PPP1CA
miR-4324	CDC25B, MAP3K3, MKNK2, PRKACA
miR-454	CDKN1A, MAP4K4, PDK1
miR-659	GSK3B, MEF2C, SOCS2
Upregulated miRNAs	*Downregulated mRNAs*
miR-1915	*PIK3R3*
miR-301a	*PRKACB, SPHK2*
miR-3190	*RPS6KB1*
miR-548h	*CCNB1,CCNG2,IL7,RPS6KA6*
miR-548m	*CCNG1*
miR-762	*CALM3*

2.5.6 PGE2-ZEB1-miR-200b-PLCG1 may represent one axis underlying the role of PGE2 in prostate cancer development and progression

miR-200b and the PLCG1 gene was among the miRNA:mRNA anticorrelated pairs we determined. This miRNA:mRNA binding had been validated in breast cancer cell lines by Dr. O Sahin's group and found to regulate cell proliferation and invasion (38); however, no study has been performed in prostate cancer cells focusing on this regulatory module. To assess their expression levels, we applied qRT-PCR to miR-200b and PLCG1 gene transcript. miR-200 a and b exhibited a 4-fold and 3-fold decrease, respectively, in PC-3/PGE2 cells, while PLCG1 possessed about 3-fold increase (Figure 2.5). Notably, the protein product of PLCG1 showed a consistent increase with its gene transcript but with a relatively lower FC of about 1.75-fold (Figure 2.6).

Similar to protein-coding genes, miRNAs are transcribed from the genome by RNA polymerase II and are subject to modulation under transcription factors.

One highlighted transcription factor which regulates the miR-200 family is ZEB1. ZEB1 and the miR-200 family are reciprocally linked in a feedback loop, which serves as a switch and activator of epithelial-to-mesenchymal transition (EMT) in development as well as in disease (39-41). Our qRT-PCR determined the mRNA level of ZEB1 increased in PC-3/PGE2 cells, which in turn, may lead to decrease of the miR-200 family (Figure 2.5); however, the increase of ZEB1 was not statistically significant after applying a t-test. This may be caused by the variation within biological triplicate, thus the experiments need to be repeated. Furthermore, PGE2 treatment increased the expression of ZEB1 in non-small lung cancer cells (39); thus the reason for increased ZEB1 in prostate cancer may be PGE2 over-production.

Collectively, we identified a decrease of miR-200b and an increase of ZEB1 and PLCG1 in the PC3/PGE2 system. One predicted regulatory axis was that PGE2 induced the expression of transcriptional repressor ZEB1. Increased ZEB1 formed a negative regulatory loop with miR-200b and decreased expression of miR-200b. Decreased miR-200b augmented the expression of PLCG1. Increased PLCG1 may contribute to downstream signaling cascades, including

PI3K and MAPK (Figure 2.5) (42-44), leading to acceleration of cell growth, proliferation, survival, and invasion. We did observe that PC-3/PGE2 cells had a higher proliferation rate compared to control PC-3 cells by MTT proliferation assay (Figure 2.7).

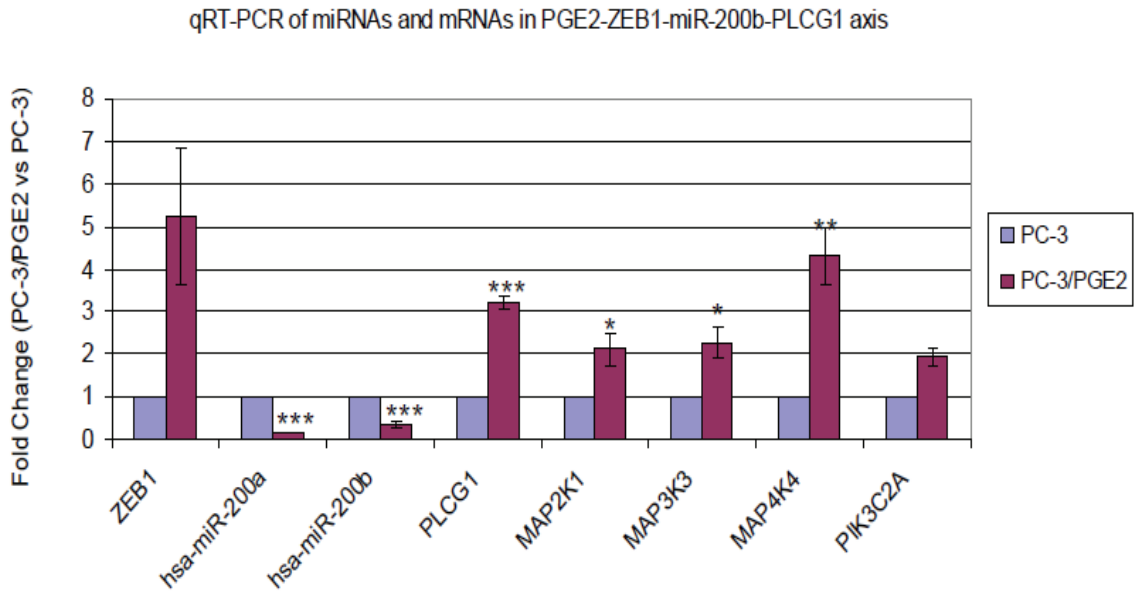

Figure 2.5: qRT-PCR validation of DE miRNAs and mRNAs implied in the proposed PGE2-ZEB1-miR-200b-PLCG1 axis

miRNA and mRNA expression in PC-3/PGE2 cells and in control PC-3 cells were quantified by qRT-PCR. U6 and RNU48 were applied as endogenous house-keeping genes for assayed miRNAs, while GAPDH and β-actin were applied for assayed mRNAs. The height of columns indicated FCs of particular miRNA or mRNA expression between PC3/PGE2 cells and control PC-3 cells (FCs were set to one). Error bars depicted SEM of three biological replicates. Significance of differences between PC-3 cells (control) and PC-3/PGE2 cells was calculated by 2-tailed Student's t-test and are represented by p-value. *** represented a p-value < 0.001, ** represented a p-value < 0.01, * represented a p-value < 0.05, and no asterisk represented no significant differences (p-value > 0.05).

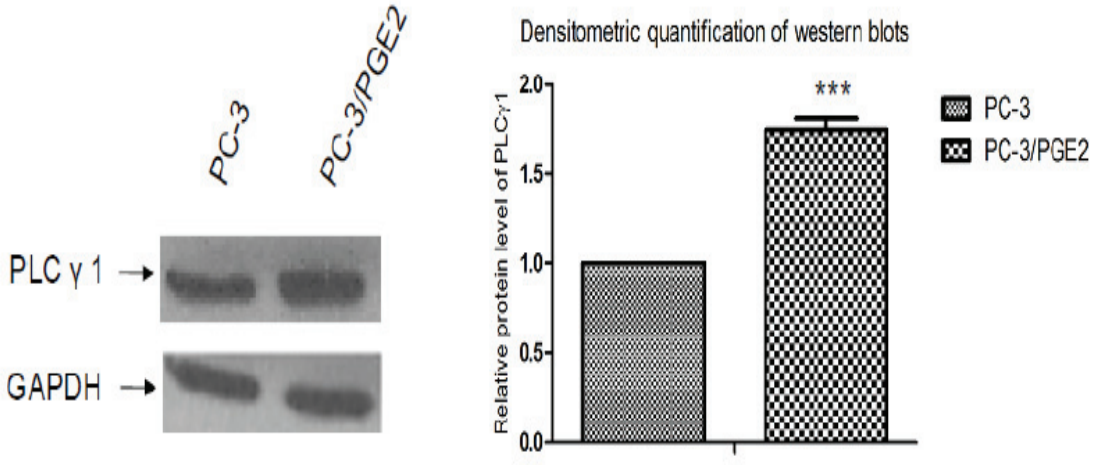

Figure 2.6: Western blots validation of PLCG1 expression in control PC-3 cells (lane 1) and PC-3/PGE2 cells (lane 2).

Protein expression of PLCG1 in PC-3 cells with excessive endogenous PGE2 (PC-3/PGE2) and in control PC-3 cells were examined by western blots. GAPDH was applied to indicate equal protein amount loaded in different lanes. Experiments were repeated 3 times. Quantification of protein levels of PLCG1 were calculated based on densitometry. Amount of PLCG1 proteins was normalized to GAPDH. Results were represented as mean ± SEM. Significance of differences between PC-3 cells (control) and PC-3/PGE2 cells was calculated by two-tailed Student's t-test and are represented by p-value. ** represented a p-value < 0.01.

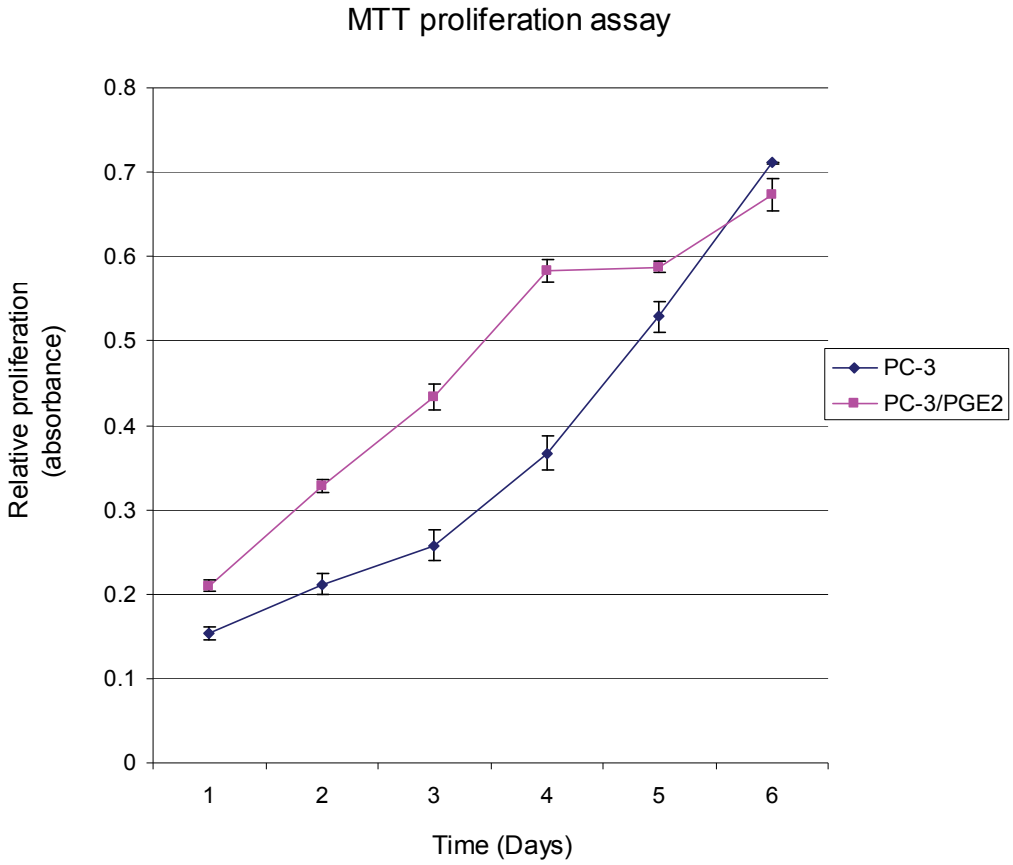

Figure 2.7: MTT proliferation assay on PC-3/PGE2 cells and control PC-3 cells

Equal number of cells was seeded into 6-well culture plates on the first day. Cells were assayed with the MTT proliferation kit (ATCC) on the subsequent day 1 to day 6, continuously. Absorbance of colorimetric signal from each well was measured at 570 nm using a microtiter plate reader. The proliferation rate of PC-3/PGE2 cells was compared with that of control cells after subtracting the intensity from no-cell blank control wells. Relative proliferation was represented by average absorbance and standard error of mean from three biological replicates.

2.6 Discussion

PGs are implicated in various types of cancers and their upstream PGES and COX enzymes are primary targets of multiple NSAIDs (nonsteroidal anti-inflammatory drugs) such as aspirin, ibuprofen, and indomethacin (17, 18). Among the PG family, PGE2, the most abundant PGs in prostate cancer, was first identified in human colon adenomas (21, 45). PGE2 and its two inducible synthases, COX-2 and mPGES-1 are increased in response to inflammation and cancer. Impaired COX-2/mPGES-1/PGE2/EP1-4 pathway in various cancers (such as breast, prostate, stomach, and pancreas cancer) can give rise to cell proliferation, invasion, adhesion, metastasis, and angiogenesis (22, 46-49). Previously, intensive studies have been carried out to investigate the PGE2 downstream molecular basis which is involved in signaling pathways and to determine the mechanism underlying its effect as a pro-inflammatory factor (17, 22).

Wang *et al*., 2007 elucidated that, in prostate cancer, PGE2 upregulated the production and secretion of VEGF through EP2 and EP4 receptors in a cAMP

dependent manner (50). Also, increased PGE2 augmented the activation of Erk1/2 and Akt; thus enhanced MAPK and PI3K/Akt signaling pathways. A similar conclusion was achieved by Jain *et al*., 2008, showing that PGE2 induced the activation of EGFR/MAPK signaling cascade and the expression of VEGF, which collectively influenced cell motility and angiogenesis in prostate cancer (22).

Another notable axis through which PGE2 exerts its effects is by transactivating EGFR/ Met receptor tyrosine kinases and ultimately triggering cell growth, invasion and migration in diverse cancer types, including hepatocellular carcinoma, colon cancer, and prostate cancer (49, 51-53). Studies applied to other cancer types demonstrated downstream modules of PGE2 included Raf/MEK/Erk, which led to increased cell proliferation; PLC/PKC/c-Src/NF-κB, which mediated cell migration; and PI3K/Akt, which controlled cell invasion and angiogenesis (25, 54, 55).

Despite the knowledge we accumulated on PGE2 in stimulating inflammation and cancer, there is no systematic profiling available regarding potential alternations

in the expression of miRNAs and gene mRNAs upon PGE2 stimulation in prostate cancer. In this study, we concomitantly profiled miRNAs and gene mRNAs in both PC-3/PGE2 cell and control PC-3 cells. The fusion recombinant enzyme expressed by COX-2-10aa-mPGES-1 plasmid mimic the biofunction of inducible COX-2 and mPGES-1 synthases which efficiently metabolize AA to produce endogenous PGE2. Once PGE2 is stimulated in prostate cancer, we identified both significant down and upregulation of miRNA expression by miRNA microarray and validated a portion of them by qRT-PCR.

Remarkably, among the downregulated miRNAs, four of them (miR-101, miR-146a, miR-200a, and miR-200b) have been previously proved to function as tumor suppressors in prostate cancer (56-58). In addition to the report of aberrant miRNA found in prostate cancer, some of decreased miRNAs in response to PGE2 are associated with other types of cancers. For instance, miR-148b is determined to suppress cancer growth and is frequently downregulated in gastric cancer and colorectal cancer (59, 60). Furthermore, miR-375 is playing a pivotal role as a tumor suppressor in diverse types of cancer, such as gastric cancer, head and neck squamous cell carcinoma (HNSCC), hepatocellular carcinoma

(HCC), and esophageal squamous cell carcinoma (ESCC) (61-65). Notably, upregulated miRNAs after PGE2 induction are poorly characterized and await further investigation.

Meanwhile, since current miRNA target prediction algorisms usually provide false positive outcomes, we combined the putative miRNA:mRNA regulatory pairs from *in silico* miRNA target prediction approach with anticorrelated miRNA:mRNA expression profiles. Therefore, we narrowed the possible altered miRNA:mRNA pairs in response to PGE2 stimulation.

Based on the comprehensive profile examination and miRNA:mRNA pairwise screening, we predicted one possible axis that may lead to overexpression of PLCG1 in PC-3/PGE2 cells. PLCG1 is critical in cancer growth, survival, invasion, and migration. It is activated by extracellular stimuli including growth factors, hormones, and neurotransmitters. Once activated, PLCG1 further catalyzes PIP2 into IP3 and DAG, whereas PLCG1 also cross talks with PI3K and MAPK signaling pathways (42-44).

At the post-transcriptional level, miR-200b potentially targeted and negatively regulated PLCG1 expression in PC-3/PGE2 cells (38). The low expression of the miR-200 family in these cells may be due to PGE2 triggered high expression of ZEB1, which acts as a transcriptional repressor to miR-200 family (39-41).

We proposed a model to show the potential regulatory mechanism of PGE2 in PC-3 cells. Besides the known signaling cascades, we predicted PGE2 may also exert its function through PGE2-ZEB1-miR-200-PLCG1 axis (Figure 2.8).

Some limitations are associated with our study. One limitation is that we did not individually examine the miRNAs and/or mRNAs which may be altered by COX-2 or mPGES-1. In our study, we applied a hybrid vector which can express a fusion protein in PC-3 cell line. This fusion protein combined COX-2 and mPGES-1 with a 10-aa linker so that it can efficiently convert endogenous AA into PGE2. We assumed that DE miRNAs/mRNAs we detected were due to upregulation of PGE2; however, this raises the possibility that differential expression may be caused by overexpression of COX-2 or mPGES-1. Moreover, miRNAs regulate mRNA transcripts of target genes at post-transcriptional level, which our

approach would not identify. Besides that, DNA methylation, transcription-factor regulation, and other forms of post-transcriptional modification are also involved in the modulation of mRNA transcripts. Thus, we present this as a preliminary study for the regulation of gene expression through miRNAs. Meanwhile, validation of interaction between DE miRNAs and their putative target mRNAs requires more intensive work.

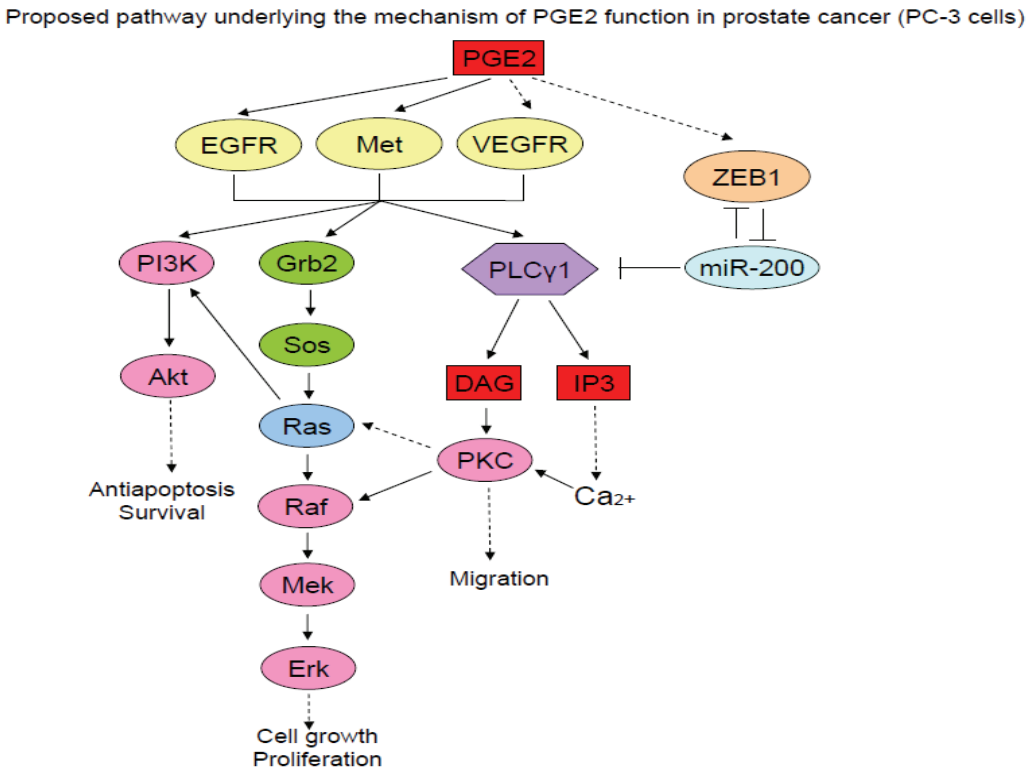

Figure 2.8: Proposed pathway underlying the mechanism of PGE2 function in prostate cancer (PC-3 cells)

PGE2 transactivates receptors including EGFR, Met, and VEGFR, which further trigger downstream signaling cascades including PI3K pathway, MAPK pathway and PKC-dependent calcium signaling pathway. One novel axis we proposed along with the existing paths is that PGE2 may induce expression of a transcriptional repressor ZEB1. ZEB1 may suppress the expression of miR-200b. Decreased level of miR-200b may lead to enhanced expression of its putative target gene, PLCG1. PLCG1 converts PIP2 into IP3 and DAG, finally resulting in the release of endogenous calcium level and the activation of subsequent calcium signaling pathway. Molecules downstream of PLCG1 also cross-talk with MAPK and PI3K pathways. Overall, the implied pathways are suggested to lead to cell growth, proliferation, migration, and survival.

2.7 Conclusion

In conclusion, we identified a subset of miRNA:mRNA pairs whose expression had been disturbed due to PGE2 upregulation in prostate cancer cells (PC-3 cells). Our findings suggested that miRNAs may play a role in negatively regulating putative target mRNA expression and thus contribute to PGE2-induced disturbances of key signaling cascades. The PGE2-ZEB1-miR-200b-PLCG1 axis, together with other unraveled PGE2-induced miRNA:mRNA pairs, may suggest a possible novel regulatory mechanism of PGs in prostate cancer. This work provide potential therapeutic candidates for the development of miRNA-based gene therapy against PGE2-associated diseases.

–

Chapter 3: MicroRNA Expression Profiling and Pathway Analysis of Porcine Adipose Tissues Revealed a Novel Potential Molecular Link Between Accumulated Body Mass, Inflammation, and Cancer

–

3.1 Key words

porcine adipose-enriched microRNA, metabolism, inflammation, cancer, miRFocus pathway enrichment analysis

3.2 Abstract

Impaired expression of miRNA is implied in various types of cancers as well as metabolic disorders, such as type II diabetes and obesity. Epidemiologic studies have revealed a strong association between body mass index (BMI) and the development of inflammatory disorders and/or cancers, yet the molecular basis of such a correlation and whether miRNAs are involved is little known. We thus set to identify novel signatures and critical predicted pathways in adipose tissues by exploring their miRNA profiles using the pigs as a model animal. Strikingly, a significant portion of identified adipose-enriched miRNAs was previously reported to be involved in metabolism, inflammatory responses, and oncogenesis. Pathway enrichment analysis provided further evidence that adipose-enriched miRNAs shared major pathways with breast cancer overexpressed miRNAs.

These findings suggested that adipose-enriched miRNAs may contribute to obesity-associated increase of cancer risk. Thus they are of high potential to serve as diagnostic and therapeutic targets for the above-mentioned diseases.

3.3 Introduction

Obesity, which is excess accumulation of adipose tissues, has dramatically increased in the past decades. Obesity has been previously demonstrated to exhibit a significant impact on the increased risk of insulin resistance, diabetes, and cardiovascular diseases (66). Recent research further elucidated that obesity is associated with the increased frequency of many common cancers, including breast cancer, prostate cancer, colon cancer, and pancreatic cancer (67). Moreover, most recent research determined that obesity may contribute to the rise in incidence of rheumatoid arthritis, which is a chronic and systematic inflammatory disorder that affects primarily the joints as well as surrounding tissues and organs (68, 69).

Obesity exerts its effect on inflammation and cancer mainly through adipocytes in adipose tissues that secrete a variety of cytokines, chemokines, growth factors, and hormones. The state of obesity accumulates more adipocytes and increases the release of inflammatory cytokines, such as TNF-α, IL-6, and PAI1 (67). Therefore, obesity itself has been recognized as a chronic, low-grade inflammatory state.

Although, epidemiologic studies have provided a positive correlation between obesity and the development of inflammatory diseases and/or cancers, the molecular-based mechanism underlying this correlation, especially on the miRNA level, is little known and awaits thorough study. In this study, we conducted miRNA profiling in a large number of tissue-specific samples obtained from six adipose depots (*i.e.,* upper and inner layers of back fat, greater omentum, mesenteric adipose, retroperitoneal adipose, and abdominal subcutaneous adipose, respectively) together with two phenotypically distinct skeletal muscle tissues (*i.e.*, longissimus dorsi muscle and psoas major muscle). Pigs were selected as the model animal for their easy-to-access feature and close phylogenetic distance to humans (70). Pigs share a similar genome size with

humans; however, their identified number of miRNAs is only ~13% (there are 255 unique mature miRNAs in pigs) to that of humans in miRBase v18 (released in November 2011). Therefore porcine miRNAome requires systemic profiling (27).

Initially, we used small RNA sequences that we identified from pigs in our previous study as candidates for microarray probe design. The probe sequences covered reported porcine miRNAs, potential novel porcine miRNAs, and their isoforms. Based on the array, we performed a systematic screening of porcine adipose and muscle tissues (71). Then from the miRNA profiles, we determined a set of miRNAs which were specifically of high-abundance in adipose tissues compared to in muscle tissues (adipose-enriched miRNAs) and further demonstrated their sequence and expression conservation in humans.

Moreover, we explored predictions related to biological function on this set of adipose-enriched miRNAs. We identified a majority of adipose-enriched miRNAs that were reported to be inflammation induced or oncogenic by published studies. Their distribution within six types of adipose tissues further differed between subcutaneous adipose tissues (SAT) (*i.e.,* upper layer of back fat, inner layer of

back fat, and abdominal subcutaneous adipose) and visceral adipose tissues (VAT) (*i.e.,* greater omentum, mesenteric adipose, retroperitoneal adipose), which suggested expression of miRNAs was highly tissue-specific.

Finally, to evaluate the global impact of adipose-enriched miRNAs and to explain the correlation between body mass index (BMI) and the risk of cancer at the scale of signaling cascades, we characterized enriched KEGG pathways of both adipose-enriched miRNAs and breast cancer overexpressed miRNAs (35-37). These findings suggested a proposed link of miRNAs that associated obesity with increased risk of cancers, and will potentially contribute to miRNA-based biomarker discovery and therapeutic intervention.

3.4 Materials and methods

3.4.1 Adipose and muscle tissues

Three female Landrace pigs (a white, Western breed) at 210-days-old were used to harvest the adipose and muscle tissues. Six adipose tissues from different body sites (*i.e.,* upper and inner layers of backfat, greater omentum, mesenteric adipose, retroperitoneal adipose, and abdominal subcutaneous adipose, respectively) together with two phenotypically distinct skeletal muscle tissues (*i.e.,* longissimus dorsi muscle and psoas major muscle) were subject to array screening.

3.4.2 Cell culture of human adipocytes

Cryopreserved human preadipocytes derived from subcutaneous and visceral depots of both lean (BMI<25.0 Kg/m2) and obese (BMI>30.0 Kg/m2) female donors. SP-F-1 were obtained from subcutaneous adipose of lean female donor and SP-F-3 were obtained from subcutaneous adipose of obese female donor.

OP-F-1 were obtained from visceral adipose of lean female donor and OP-F-3 were obtained from visceral adipose of obese female donor (Zen-Bio, Inc.). All four kinds of human adipocytes were employed for the conservation analysis of porcine miRNAs. Preadipocytes were plated into 6-well plates and cultured in preadipocyte medium (OM-PM; Zen-Bio, Inc.) at 37ºC with 5% CO_2. After plating cells for 24 hours, they became confluent and thus were ready for differentiation induction using differentiation medium (DM; Zen-Bio, Inc.) which contained isobutylmethylxanthine (0.20 mM) and PPARγ agonist (10 μM). Seven days after differentiation, the medium was again switched to adipocyte medium (AM; Zen-Bio, Inc.) specially composed of biotin (33 μM), pantothenate (17 μM), human insulin (100 nM), and dexamethasone (1 μM). Fourteen days after differentiation, cells assumed a round shape with large oil droplets in the cytoplasm and were considered as mature adipocytes, hence were suitable for RNA extraction. All four adipocyte primary cell cultures were performed in biological triplicate.

3.4.3 Cell culture of human cell lines

Human cell lines were obtained from the American Type Culture Collection (Rockville, MD). The non-tumorigenic human mammary epithelial cell line, MCF-10A, was maintained in 1:1 mixture of DMEM and Ham's F-12 medium (Invitrogen, 11885 and 11765) supplemented with 5% fetal bovine serum (FBS, Sigma, F2442), 10 µg/ml insulin, 20 ng/ml epidermal growth factor, and 0.5 ng/ml hydrocortisone (Sigma). Breast cancer T47D cells were cultured in DMEM/Ham's F-12 medium (1:1) with 5% FBS and MCF-7 cells were cultured in DMEM medium with 5% FBS. All applied culture medium contained 1% penicillin/streptomycin.

3.4.4 Total RNA extraction

Total RNA from porcine tissue samples and human adipose primary cell cultures were extracted and purified with *mirVana*™ miRNA isolation kit (Ambion) according to the manufacturer's specifications. RNA concentration was estimated

by NanoDrop ND-1000 spectrophotometer (Nano Drop) and RNA integrity was evaluated by Agilent 2100 Bioanalyzer (Agilent Technologies).

3.4.5 miRNA microarray design

Innovative probe design pipeline started with existing sequenced sequences (sequ-seqs) generated by Illumina high-throughput small RNA sequencing technology as probe candidates. In particular, 10 small RNA sequ-seq libraries obtained by Li *et al*. (2010), which represented the full porcine lifespan and were derived from 60 tissues of both sexual traits, were employed for initial probe design (71). Mammalian miRNAs collected from miRBase v15 were determined as templates (reference miRNA sequences). Considering the heterogeneous distribution of sequ-seqs to templates, probes were designed to cover 13 mammalian species (Figure 3.1). A subset of sequ-seqs, which did not map to known mammalian miRNAs, was also grouped into the probe pool for discovery profiling (they are referred to as PCC probes). Final probe content consisted of 1,572 unique experimental sequences representing a comprehensive repertoire of mammalian known miRNAs, potential novel miRNAs and their statistically

significant isoforms derived from sequ-seqs. Microarray layout was designed to contain three technical replicates for each experimental sequence. It also incorporated control probes to closely monitor microarray synthesis and sample processing quality (72, 73).

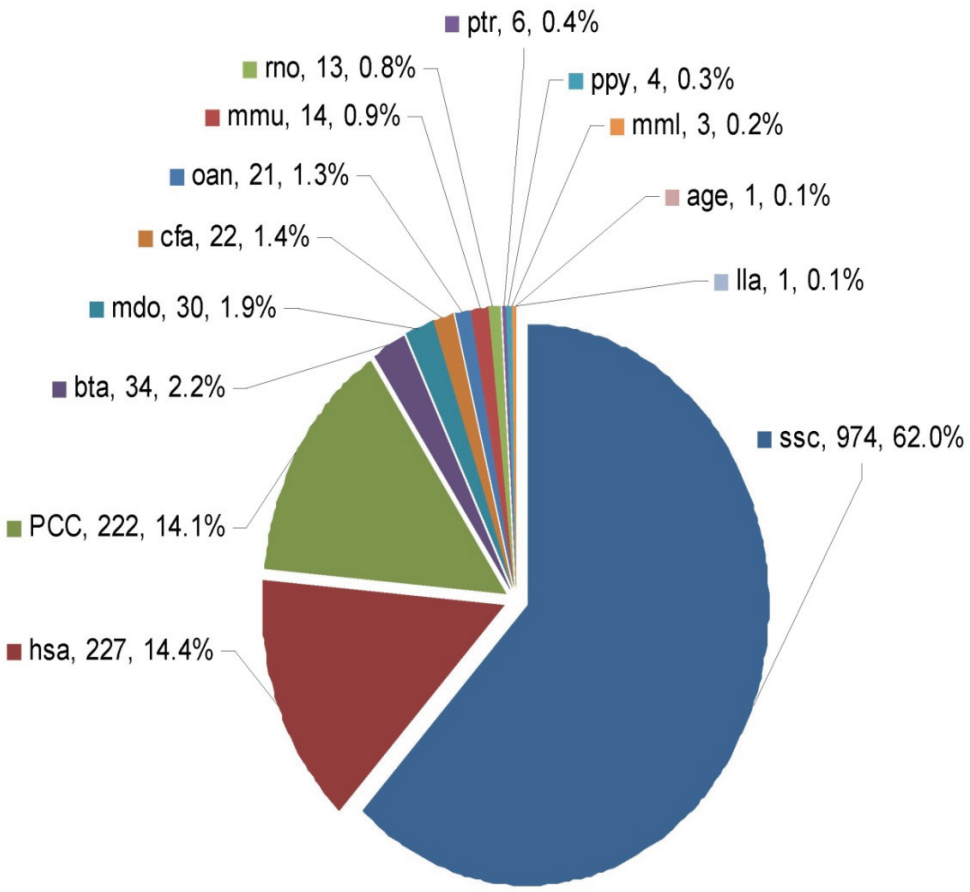

Figure 3.1: Species coverage and distribution of miRNA microarray probes

Probes were designed to cover 13 mammalian species. The largest portion of probes was intended to profile porcine miRNAs. PCC represented probes for potential novel miRNAs from sequencing reads (our candidate sequences for array probe design) which can not be mapped to mature miRNA sequences of any mammalian species. The data labels indicated "species, number of probes, and percentage to total probes". Abbreviations for species: *Sus scrofa*, ssc; *Homo sapiens*, hsa; *Bos taurus*, bta; *Monodelphis domestica*, mdo; *Canis familiaris*, cfa; *Ornithorhynchus anatinus*, oan; *Mus musculus*, mmu; *Rattus norvegicus*, rno; *Pan troglodytes*, ptr; *Pongo pygmaeus*, ppy; *Macaca mulatta*, mml; *Lagothrix lagotricha*, lla; and *Ateles geoffroyi*, age.

3.4.6 miRNA microarray profiling

About 0.5 μg of total RNA was 3' dephosphorylated by Antarctic phosphatase (New England Biolabs, Catalog No. M0289S) and purified by RNeasy MiniElute Cleanup Kit (Qiagen, Catalog No. 74204). Specific oligonucleotide adaptors were ligated to the 3' of RNA and followed by fluorescent dendrimer-dye conjugation. Tagged RNA samples were hybridized on a μParaflo microfluidic chip at 40 °C for 16 hours using a micro-circulation hybridization station (LC Sciences). Subsequently, Alexa Fluor® 3 dyes (Invitrogen) were circulated to samples for staining at 34 °C for 2 hours. Array images were acquired on a GenePix 4400B laser scanner (Molecular Device) in 532 nm channel. Images were first digitalized with Array-Pro Analyzer (MediaCybernetics) to quantify signal mean and standard deviation of each probe spot on the array surface. Profilings were performed using three biological replicates from three individual pigs.

3.4.7 miRNA microarray data analysis

Microarray data were further processed by background subtraction and LOWESS (locally weighted regression) normalization so that biological variations between samples could be identified. Significance of differences between porcine adipose and muscle miRNA profiles was analyzed by Student *t*-test with $p < 0.01$, 0.05, or 0.1 respectively (72). Heatmap and clustering of differentially expressed (DE) miRNAs were generated by MeV software (The Institute for Genome Research).

3.4.8 miRNA Illumina sequencing

Six different adipose tissues and two skeletal muscle tissues from three female Landrace pigs were employed for small RNA sequencing. For each sequencing sample, equal quantities (5 µg) of small RNA isolated from three female Landrace pigs were pooled. Approximately 15 µg of small RNA representing each tissue was used for subsequent library preparation and sequencing according to Illumina's manufacturer protocols. The reads were first passed

through the filters of Illumina's Genome Analyzer Pipeline software and then were subject to the in-house developed ACGT101 program, where reads were counted, grouped into sequence families, and mapped to available mammalian miRNAs in miRBase v15 (71, 73).

3.4.9 qRT-PCR

Ten adipose-enriched miRNAs derived from porcine adipose tissues were validated in human adipocyte primary cell cultures by qRT-PCR using NCode™ EXPRESS SYBR® GreenER™ miRNA kit (Invitrogen) on an ABI 7900HT instrument (Applied Biosystems) according to manufacturers' protocols. Sequences of miRNA specific forward primers and RNU48 endogenous control primer were provided in Table 3.1. The ΔΔCt method was applied to calculate FC of surveyed adipose abundant miRNAs. Corresponding miRNA expression in human muscles was considered as reference. The relative FCs for each miRNA were plotted and error bar indicated SEM from three biological replicates.

Table 3.1: PCR primers used in the qRT-PCR validation assays

miRNA	Primer
ssc-miR-103	CAGCATTGTACAGGGCTATGA
ssc-miR-107	CAGCATTGTACAGGGCTATCA
ssc-miR-130a	CAGTGCAATGTTAAAAGGGCAT
ssc-miR-143	GGTGAGATGAAGCACTGTAGCTC
ssc-miR-148a	GCTCAGTGCACTACAGAACTTTGT
ssc-miR-193a-5p	GCGGGCGAGATGAAAAA
ssc-miR-199a-5p	CCCAGTGTTCAGACTACCTGTTC
hsa-miR-200b	GGTAATACTGCCTGGTAATGATGA
hsa-miR-221	AGCTACATTGTCTGCTGGGTTTC
RNU48	AGTGATGATGACCCCAGGTAACTC

3.4.10 miRNA pathway enrichment analysis

Enriched biological pathways associated with a set of miRNAs were investigated with miRFocus (http://www.mirfocus.org/), an open resource web-tool. First, putative miRNA target genes were retrieved and merged from 5 target prediction algorithms: MiRanda (http://www.microrna.org), MirTarget2 (miRDB: http://mirdb.org), PicTar (http://pictar.mdc-berlin.de), TargetScan (http://www.targetscan.org) and DIANA microT (http://diana.cslab.ece.ntua.gr/microT) (33, 74-80); together with 4 validated miR-target gene databases: MiRecord (http://mirecords.biolead.org), miR2Disease (http://www.mir2disease.org), TarBase (http://diana.cslab.ece.ntua.gr/tarbase) and miRTarbase (http://mirtarbase.mbc.nctu.edu.tw) (81-84). To enhance the accuracy and reliability of target prediction, common target genes shared by at least 3 algorithms were selected into target pool. Then, the target pool of input miRNAs was mapped to KEGG database in order to identify enriched biological pathways (35-37). The significance of each pathway was assessed by Fisher's exact test and represented by *p*-value.

3.5 Results and discussion

3.5.1 Identification and validation of adipose-enriched miRNAs

To systematically identify miRNAs which were universally enriched in porcine adipose tissues, we profiled miRNA expression of adipose tissues from six different fat depots (upper and inner layers of back fat, greater omentum, mesenteric adipose, retroperitoneal adipose, and abdominal subcutaneous adipose) together with muscle tissues from two muscle depots (longissimus dorsi muscle and psoas major muscle) using a high-definition miRNA microarray approach.

As shown in Table 3.4, out of 1,572 unique probes, 56 miRNAs exhibited distinct expression patterns between the two types of tissues after student t-test with *p*-value < 0.05 (Table 3.2 and Table 3.3). Among them, 32 miRNAs (including miR-103a, miR-107, miR-122, miR-146, and miR-21) were highly expressed in adipose tissues; while in contrast, 24 miRNAs (including miR-1, miR-128, miR-

133, miR-181, and miR-193) were highly expressed in muscle tissues (Table 3.4 and Figure 3.2).

We further compared out miRNA microarray results to that of Illumina small RNA sequencing (NGS) using the exactly same set of porcine tissue samples. Copy number of sequenced-sequences (sequ-seqs) satisfying quality criterias were compared to the probe intensity from microarray of the same miRNA. In Figure 3.3, we evaluated reproducibility and correlation between the two platforms by computing the FC ratios of miRNA expression between the two types of tissues. We determined that Person correlation coefficient (r) between NGS and microarray on the 56 miRNAs determined as DE by microarray was 0.88, supporting the reproducibility and reliability of our miRNA microarray data.

Table 3.2: miRNAs highly expressed in porcine adipose tissues

Index	miRNA ID	Expression in adipose tissues	Expression in muscle tissues	Log2(FC)	*p*-value	Significance label
1	hsa-let-7b	3,261	1,603	1.02	1.10E-02	**
2	ssc-let-7c	6,544	3,512	0.90	2.30E-03	***
3	ssc-let-7i	3,694	2,189	0.75	2.50E-02	**
4	bta-miR-21	12,967	7,305	0.83	2.03E-02	**
5	ssc-miR-100	7,080	4,393	0.69	3.78E-04	***
6	ssc-miR-103	3,263	1,049	1.64	8.73E-03	***
7	ssc-miR-107	3,483	981	1.83	4.06E-06	***
8	ssc-miR-122	83	3	5.03	2.82E-02	**
9	ssc-miR-130a	1,735	532	1.71	1.35E-06	***
10	ssc-miR-140*	1,017	309	1.72	6.92E-04	***
11	ssc-miR-143	6,965	2,755	1.34	2.87E-03	***
12	ssc-miR-145	19,044	8,491	1.17	1.28E-03	***
13	mmu-miR-145*	434	89	2.29	5.74E-04	***
14	hsa-miR-146a	2,753	484	2.51	9.85E-03	***
15	ssc-miR-146b	230	55	2.06	1.10E-02	**
16	ssc-miR-148a	9,529	2,453	1.96	6.05E-04	***
17	ssc-miR-152	2,827	977	1.53	1.94E-03	***
18	mmu-miR-155	838	78	3.43	1.57E-06	***
19	ssc-miR-185	330	122	1.44	2.64E-02	**
20	ssc-miR-193a-3p	812	249	1.70	2.40E-02	**
21	ssc-miR-193a-5p	1,177	265	2.15	1.86E-04	***
22	ssc-miR-199a-3p	8,795	2,721	1.69	1.79E-02	**
23	ssc-miR-199a-5p	7,613	2,663	1.52	4.82E-05	***
24	hsa-miR-199b-5p	2,566	1,127	1.19	5.48E-03	***
25	ssc-miR-199b*	10,467	2,860	1.87	1.33E-02	**
26	hsa-miR-200a	1,150	8	7.23	6.17E-03	***
27	hsa-miR-200b	897	5	7.35	2.75E-03	***
28	hsa-miR-203	611	94	2.71	1.95E-07	***
29	hsa-miR-221	1,023	145	2.82	9.25E-06	***
30	hsa-miR-320b	1,964	808	1.28	3.23E-04	***
31	hsa-miR-320d	1,018	508	1.00	4.85E-03	***
32	hsa-miR-375	916	3	8.33	3.30E-02	**

Table 3.3: miRNAs highly expressed in porcine muscle tissues

Index	miRNA ID	Expression in adipose tissues	Expression in muscle tissues	Log2(FC)	*p*-value	Significance label
1	hsa-let-7d*	179	431	-1.26	1.10E-03	***
2	oan-let-7e	250	2,693	-3.43	5.84E-03	***
3	ssc-miR-1	32	79,491	-11.29	1.24E-14	***
4	ssc-miR-15a	2,797	7,544	-1.43	1.11E-09	***
5	ssc-miR-19b	2,057	3,526	-0.78	8.03E-04	***
6	cfa-miR-20b	321	515	-0.68	4.40E-03	***
7	hsa-miR-26b	4,560	8,845	-0.96	1.46E-03	***
8	hsa-miR-28-5p	661	3,273	-2.31	2.13E-06	***
9	ssc-miR-101	1,858	5,670	-1.61	3.73E-08	***
10	ssc-miR-106a	760	1,175	-0.63	6.61E-03	***
11	ssc-miR-128	326	8,706	-4.74	5.47E-10	***
12	ssc-miR-133a	131	52,089	-8.63	1.27E-14	***
13	ssc-miR-133b	250	59,388	-7.89	1.80E-14	***
14	ssc-miR-151-3p	303	940	-1.63	2.39E-03	***
15	ssc-miR-151-5p	2,880	8,333	-1.53	1.96E-03	***
16	ssc-miR-181a	2,153	3,303	-0.62	4.41E-02	**
17	bta-miR-193b	1,556	6,374	-2.03	2.24E-05	***
18	ssc-miR-196a	99	176	-0.83	5.02E-04	***
19	ssc-miR-196b	138	144	-0.07	1.40E-02	**
20	ssc-miR-206	17	18,417	-10.09	1.62E-10	***
21	hsa-miR-362-3p	163	400	-1.30	3.77E-03	***
22	hsa-miR-362-5p	156	301	-0.95	4.54E-02	**
23	hsa-miR-376c	129	403	-1.64	1.39E-05	***
24	hsa-miR-487b	128	453	-1.83	1.39E-03	***

Note: Log2(FC) calculated as log2(miRNA expression in adipose/expression in muscle)
Significance label: *** p-value<0.001, ** p-value<0.01

Table 3.4: DE miRNAs between porcine adipose and muscle tissues

Adipose-enriched miRNAs			Muscle-enriched miRNAs		
miRNA ID	Log2Ratio[#]	*p*-value	miRNA ID	Log2Ratio[#]	*p*-value
hsa-let-7b	1.02	**	hsa-let-7d*	-1.26	***
ssc-let-7c	0.90	***	oan-let-7e	-3.43	***
ssc-let-7i	0.75	**	ssc-miR-1	-11.29	***
bta-miR-21	0.83	**	ssc-miR-15a	-1.43	***
ssc-miR-100	0.69	***	ssc-miR-19b	-0.78	***
ssc-miR-103	1.64	***	cfa-miR-20b	-0.68	***
ssc-miR-107	1.83	***	hsa-miR-26b	-0.96	***
ssc-miR-122	5.03	**	hsa-miR-28-5p	-2.31	***
ssc-miR-130a	1.71	***	ssc-miR-101	-1.61	***
ssc-miR-140*	1.72	***	ssc-miR-106a	-0.63	***
ssc-miR-143	1.34	***	ssc-miR-128	-4.74	***
ssc-miR-145	1.17	***	ssc-miR-133a	-8.63	***
mmu-miR-145*	2.29	***	ssc-miR-133b	-7.89	***
hsa-miR-146a	2.51	***	ssc-miR-151-3p	-1.63	***
ssc-miR-146b	2.06	**	ssc-miR-151-5p	-1.53	***
ssc-miR-148a	1.96	***	ssc-miR-181a	-0.62	**
ssc-miR-152	1.53	***	bta-miR-193b	-2.03	***
mmu-miR-155	3.43	***	ssc-miR-196a	-0.83	***
ssc-miR-185	1.44	**	ssc-miR-196b	-0.07	**
ssc-miR-193a-3p	1.70	**	ssc-miR-206	-10.09	***
ssc-miR-193a-5p	2.15	***	hsa-miR-362-3p	-1.30	***
ssc-miR-199a-3p	1.69	**	hsa-miR-362-5p	-0.95	**
ssc-miR-199a-5p	1.52	***	hsa-miR-376c	-1.64	***
hsa-miR-199b-5p	1.19	***	hsa-miR-487b	-1.83	***
ssc-miR-199b*	1.87	**			
hsa-miR-200a	7.23	***			
hsa-miR-200b	7.35	***			
hsa-miR-203	2.71	***			
hsa-miR-221	2.82	***			
hsa-miR-320b	1.28	***			
hsa-miR-320d	1.00	***			
hsa-miR-375	8.33	**			

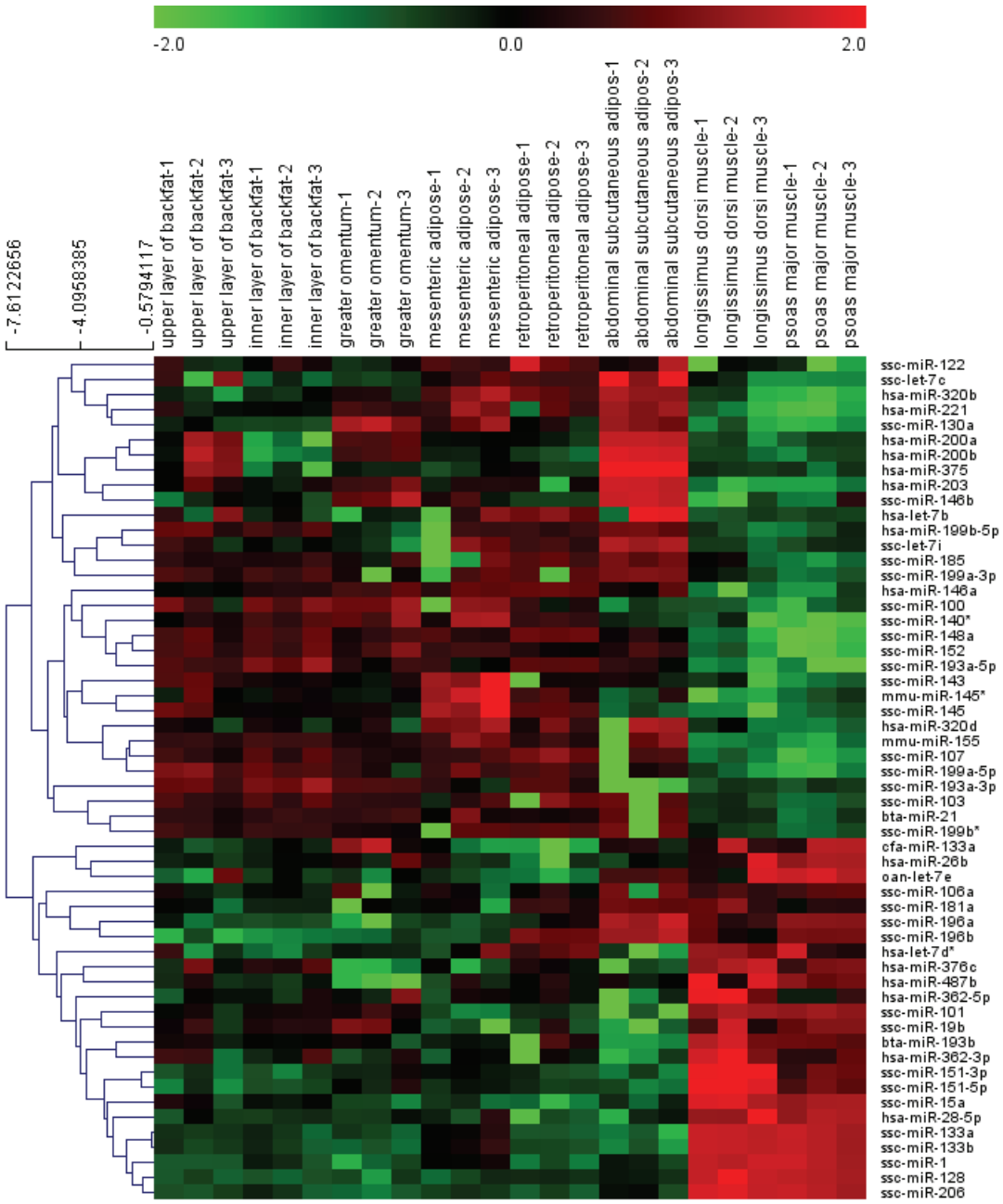
-2.0
0.0
2.0
-7.6122656
-4.0958385
-0.5794117
upper layer of backfat-1
upper layer of backfat-2
upper layer of backfat-3
inner layer of backfat-1
inner layer of backfat-2
inner layer of backfat-3
greater omentum-1
greater omentum-2
greater omentum-3
mesenteric adipose-1
mesenteric adipose-2
mesenteric adipose-3
retroperitoneal adipose-1
retroperitoneal adipose-2
retroperitoneal adipose-3
abdominal subcutaneous adipos-1
abdominal subcutaneous adipos-2
abdominal subcutaneous adipos-3
longissimus dorsi muscle-1
longissimus dorsi muscle-2
longissimus dorsi muscle-3
psoas major muscle-1
psoas major muscle-2
psoas major muscle-3
ssc-miR-122
ssc-let-7c
hsa-miR-320b
hsa-miR-221
ssc-miR-130a
hsa-miR-200a
hsa-miR-200b
hsa-miR-375
hsa-miR-203
ssc-miR-146b
hsa-let-7b
hsa-miR-199b-5p
ssc-let-7i
ssc-miR-185
ssc-miR-199a-3p
hsa-miR-146a
ssc-miR-100
ssc-miR-140*
ssc-miR-148a
ssc-miR-152
ssc-miR-193a-5p
ssc-miR-143
mmu-miR-145*
ssc-miR-145
hsa-miR-320d
mmu-miR-155
ssc-miR-107
ssc-miR-199a-5p
ssc-miR-193a-3p
ssc-miR-103
bta-miR-21
ssc-miR-199b*
cfa-miR-133a
hsa-miR-26b
oan-let-7e
ssc-miR-106a
ssc-miR-181a
ssc-miR-196a
ssc-miR-196b
hsa-let-7d*
hsa-miR-376c
hsa-miR-487b
hsa-miR-362-5p
ssc-miR-101
ssc-miR-19b
bta-miR-193b
hsa-miR-362-3p
ssc-miR-151-3p
ssc-miR-151-5p
ssc-miR-15a
hsa-miR-28-5p
ssc-miR-133a
ssc-miR-133b
ssc-miR-1
ssc-miR-128
ssc-miR-206

Figure 3.2: Heatmap and hierarchical clustering of DE miRNA expression in adipose and muscle tissues

z-scores ($z = (x - \mu) / \sigma$, x = raw score or observation to be standardized, μ = mean of the population, and σ = standard deviation of the population) from 24 normalized miRNA microarray data sets were hierarchically clustered in gene dimension and plotted as a heat map. t-test was performed between 6 types of adipose samples (left) and 2 types muscle samples (right). Each type of samples contained three biological replicates. Probes with *p*-value <0.05 after t-test were presented in the plot. Dendrograms on the left side indicated the euclidean distance among miRNAs. Red and Green color denoted z-scores ranging from -2.0to 0 to +2.0. Red represented high expression levels and green low expression. Detailed expression and ratio changes of miRNAs were shown in Table 3.2, Table 3.3, and Table 3.4.

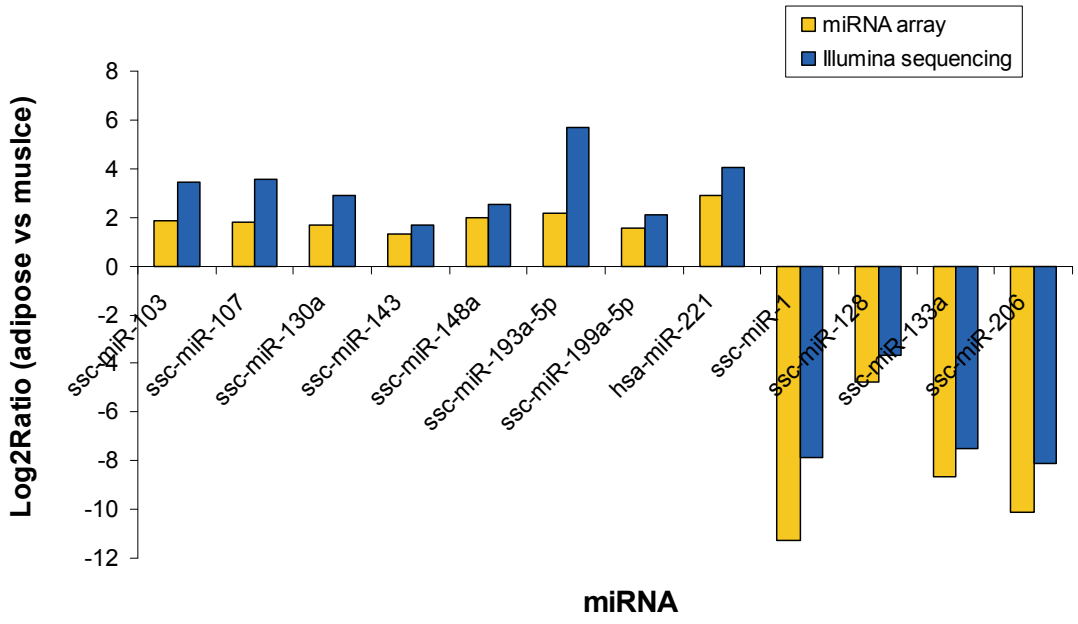

Figure 3.3: Validation of DE miRNA obtained from microarray by Illumina small RNA sequencing

miRNA expression FCs were computed either based on intensity as generated from microarray or based on miRNA copy number as determined from Illumina small RNA sequencing. The y-axis represented the log2 transformed FC between adipose tissues and muscle tissues of 12 DE miRNAs (shown in x-axis). Tested DE miRNAs exhibited consistent high expression in adipose tissues or in muscle tissues within the two platforms we used and thus we validated the microarray data we obtained.

3.5.2 Porcine adipose-enriched miRNAs were conserved in human

To date, 255 mature porcine miRNA sequences have been identified and deposited to miRBase v18 (released in November 2011) (27); however, rarely have any functional and pathway annotations been unraveled of biomedical interest (73, 85, 86). The poorly studied porcine miRNAome requires comparative studies between porcine and human miRNAs (87).

In order to apply our accumulated knowledge of human miRNAs to the porcine adipose-enriched miRNAs we obtained, we first aligned and compared sequences of porcine adipose-enriched miRNAs, which were assessed from complimentary of their corresponding microarray probe sequences, with their human orthologs. Results in Table 3.5 provided us with evidence that sequences between porcine adipose-enriched miRNAs and their human orthologs were either identical or highly conserved, with only one to two-nucleotide differences at

5' and/or 3' end, which was not the critical position for miRNAs to exert their biological function.

Moreover, expression of corresponding human orthologs to porcine adipose-enriched miRNAs was determined by qRT-PCR approach. We examined four kinds of human adipocytes (as shown in different colors in Figure 3.4) sourced from either subcutaneous or omental depot of both lean (BMI<25.0 Kg/m^2) and obese (BMI>30.0 Kg/m^2) female donors. Relative expression of each miRNA in human adipocytes versus in human muscles was presented as FCs in y-axis. Based on the expression patterns of miRNAs, we concluded that porcine adipose-enriched miRNAs exhibited consistent high expression in human adipocytes but not in human muscles.

Overall, we confirmed that both sequences and expression of miRNAs in pigs were conserved in humans, which were consistent with the close phylogenetic distance between pigs and humans and further suggested the pigs as a valuable animal model for biomedical research.

Table 3.5: Comparison of sequences of porcine adipose-enriched miRNAs with their human orthologs

Index	Probe miRNA ID	Probe sequences	Human ortholog sequences	Human miRNA ID
1	hsa-let-7b	TGAGGTAGTAGGTTGTGTGGTT	TGAGGTAGTAGGTTGTGTGGTT	hsa-let-7b
2	ssc-let-7c	TGAGGTAGTAGGTTGTATGGTT	TGAGGTAGTAGGTTGTATGGTT	hsa-let-7c
3	ssc-let-7i	TGAGGTAGTAGTTTGTGCT	TGAGGTAGTAGTTTGTGCTGTT	hsa-let-7i
4	bta-miR-21	TAGCTTATCAGACTGATGTTGACT	TAGCTTATCAGACTGATGTTGA	hsa-miR-21
5	ssc-miR-100	AACCCGTAGATCCGAACTTGTG	AACCCGTAGATCCGAACTTGTG	hsa-miR-100
6	ssc-miR-103	AGCAGCATTGTACAGGGCTATGA	AGCAGCATTGTACAGGGCTATGA	hsa-miR-103a
7	ssc-miR-107	AGCAGCATTGTACAGGGCTATCA	AGCAGCATTGTACAGGGCTATCA	hsa-miR-107
8	ssc-miR-122	TGGAGTGTGACAATGGTGTTTGT	TGGAGTGTGACAATGGTGTTTG	hsa-miR-122
9	ssc-miR-130a	CAGTGCAATGTTAAAAGGGCAT	CAGTGCAATGTTAAAAGGGCAT	hsa-miR-130a
10	ssc-miR-140*	TACCACAGGGTAGAACCACGGAC	TACCACAGGGTAGAACCACGG	hsa-miR-140-3p
11	ssc-miR-143	TGAGATGAAGCACTGTAGCTC	TGAGATGAAGCACTGTAGCTC	hsa-miR-143
12	ssc-miR-145	GTCCAGTTTTCCCAGGAATCCCTT	GTCCAGTTTTCCCAGGAATCCCT	hsa-miR-145
13	mmu-miR-145*	ATTCCTGGAAATACTGTTCTTG	GGATTCCTGGAAATACTGTTCT	hsa-miR-145*
14	hsa-miR-146a	TGAGAACTGAATTCCATGGGTT	TGAGAACTGAATTCCATGGGTT	hsa-miR-146a
15	ssc-miR-146b	TGAGAACTGAATTCCATAGGC	TGAGAACTGAATTCCATAGGCT	hsa-miR-146b-5p
16	ssc-miR-148a	TCAGTGCACTACAGAACTTTGT	TCAGTGCACTACAGAACTTTGT	hsa-miR-148a
17	ssc-miR-152	TCAGTGCATGACAGAACTTGG	TCAGTGCATGACAGAACTTGG	hsa-miR-152
18	mmu-miR-155	TTAATGCTAATTGTGATAGGGGT	TTAATGCTAATCGTGATAGGGGT	hsa-miR-155
19	ssc-miR-185	TGGAGAGAAAGGCAGTTCCTGA	TGGAGAGAAAGGCAGTTCCTGA	hsa-miR-185
20	ssc-miR-193a-3p	ACAGTAGTCTGCACATTGGTTA	ACAGTAGTCTGCACATTGGTTA	hsa-miR-193a-3p
21	ssc-miR-193a-5p	TGGGTCTTTGCGGGCGAGATGA	TGGGTCTTTGCGGGCGAGATGA	hsa-miR-193a-5p
22	ssc-miR-199a-3p	ACAGTAGTCTGCACATTGGTTA	ACAGTAGTCTGCACATTGGTTA	hsa-miR-199a-3p
23	ssc-miR-199a-5p	CCCAGTGTTCAGACTACCTGTTC	CCCAGTGTTCAGACTACCTGTTC	hsa-miR-199a-5p
24	hsa-miR-199b-5p	CCCAGTGTTTAGACTATCTGTTC	CCCAGTGTTTAGACTATCTGTTC	hsa-miR-199b-5p
25	ssc-miR-199b*	TACAGTAGTCTGCACATTGGTT	ACAGTAGTCTGCACATTGGTTA	hsa-miR-199b-3p
26	hsa-miR-200a	TAACACTGTCTGGTAACGATGT	TAACACTGTCTGGTAACGATGT	hsa-miR-200a
27	hsa-miR-200b	TAATACTGCCTGGTAATGATGA	TAATACTGCCTGGTAATGATGA	hsa-miR-200b
28	hsa-miR-203	GTGAAATGTTTAGGACCACTAG	GTGAAATGTTTAGGACCACTAG	hsa-miR-203
29	hsa-miR-221	AGCTACATTGTCTGCTGGGTTTC	AGCTACATTGTCTGCTGGGTTTC	hsa-miR-221
30	hsa-miR-320b	AAAAGCTGGGTTGAGAGGGCAA	AAAAGCTGGGTTGAGAGGGCAA	hsa-miR-320b
31	hsa-miR-320d	AAAAGCTGGGTTGAGAGGA	AAAAGCTGGGTTGAGAGGA	hsa-miR-320d
32	hsa-miR-375	TTTGTTCGTTCGGCTCGCGTGA	TTTGTTCGTTCGGCTCGCGTGA	hsa-miR-375

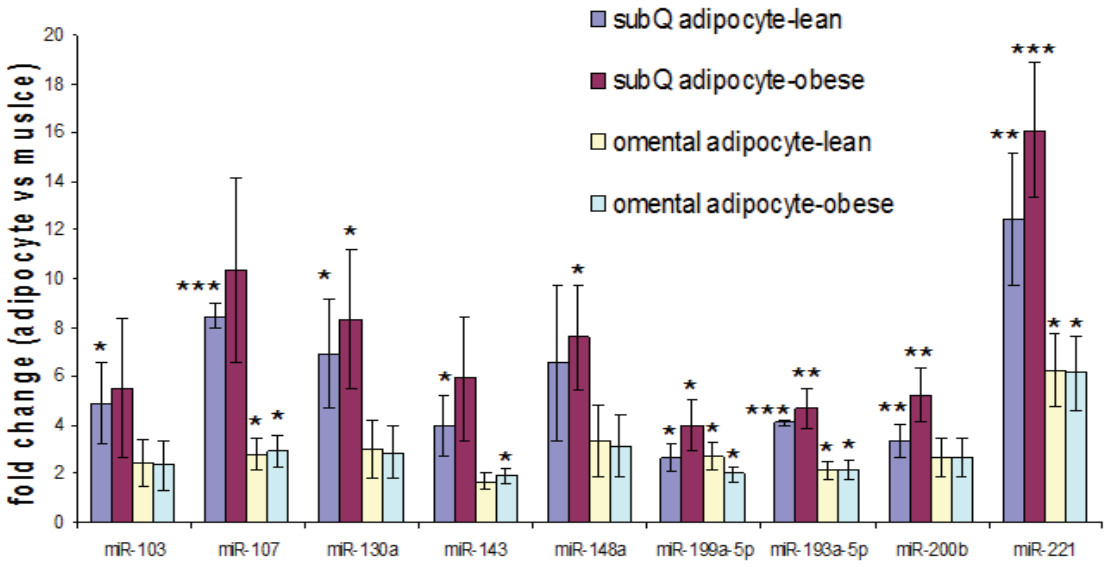

Figure 3.4: Quantification of the expression of porcine adipose-enriched miRNAs in human adipocytes by qRT-PCR approach

Expression of 9 adipose-enriched miRNAs originally identified from pigs was examined in human adipocytes using qRT-PCR. RNU48 snRNA was used as endogenous control and its expression was uniform across all human samples. Expression of miRNA was first normalized to endogenous control. Then FCs of miRNA expression between adipocytes and muscles were calculated by the ΔΔCt method. Columns of different colors represented 4 kinds of human adipocytes obtained from subcutaneous and omental depots of both lean (BMI<25.0 kg/m^2) and obese (BMI>30.0 kg/m^2) female donors. The height of columns indicated FCs of miRNA expression between human adipocytes and muscles. Data was expressed as mean ± SEM (n=3 biological replicates). Significance of differences was calculated by two-tailed Student's t-test and are represented by *p*-value. *** represented a *p*-value < 0.001, ** represented a *p*-value < 0.01, * represented a *p*-value < 0.05, no asterisk represented no significant differences (*p*-value > 0.05).

3.5.3 Adipose-enriched miRNAs were involved in metabolism

Adipose tissues are the largest energy reservoir for triglycerides. Mature adipocytes, the major cell type of adipose tissues, uptake glycerol and fatty acid and synthesize them into triglyceride (lipogenesis). The store of triglycerides can be hydrolysed to release fatty acid into body circulation (lipolysis) (88). Insulin plays a crucial role in lipid metabolism by promoting glucose uptake which is followed by lipogenesis, and inhibiting lipolysis (89). Dysregulation of energy deposition in adipose tissue, for instance, obesity, will lead to insulin-related disorders, such as insulin resistance and type 2 diabetes (88).

Due to the function of adipose tissues in lipid and glucose metabolism, we determined that a set of adipose-enriched miRNAs (5 out of 32) were involved in metabolic processes in different types of tissues and/or cells as reported by published studies. For example, miR-103/107 mediates insulin sensitivity and control glucose homeostasis in mouse liver(12); miR-122, which is the most

prevalent miRNA in liver and is conserved among multiple species, controls cholesterol accumulation in mouse liver (13); miR-143 regulates lipid metabolism in liver and its expression is induced by obesity. Upregulated miR-143 impairs glucose homeostasis (14); miR-375 mediates glucose regulation of insulin gene expression and β cell growth in pancreas (15).

Notably, the distribution and expression of metabolism related adipose-enriched miRNAs varied among the six adipose depots (Table 3.6). Their expression was consistently higher in adipose tissues than in muscle tissues, among them, miR-107 was further enriched in retroperitoneal adipose, miR-143 in mesenteric adipose, and miR-375 in abdominal subcutaneous adipose.

To sum up, adipose tissue, as a type of active tissue for body metabolism, contains highly expressed miRNAs (adipose-enriched miRNAs) which are reported to be implicated in energy homeostasis, glucose, and lipid regulation in different biological systems. Distorted expression of those miRNAs is implied in metabolic syndromes and diseases. Elucidation of their role in adipose tissue

may provide opportunity for better diagnosis, prognosis, and therapeutic intervention of obesity, diabetes, and other metabolic disorders.

Table 3.6: Relative expression of adipose-enriched miRNAs among 6 adipose depots

miRNA ID	Description	SAT			VAT		
		upper layer of backfat	inner layer of backfat	abdominal subcutaneous	greater omentum	mesenteric adipose	retroperitoneal adipose
miR-103	metabolism, oncogenic						
miR-107							
miR-122							
miR-143	metabolism						
miR-375							
miR-21	inflammation, oncogenic						
miR-146a							
miR-155							
miR-193a-3p	tumor suppressor						
miR-193a-5p							
miR-200a							
miR-200b							
miR-100	oncogenic						
miR-130							
miR-140							
miR-148							
miR-199							
miR-221							

Note: Red indicates high expression level which is above the mean of all the 6 adipose depots and green low expression. Grey represents average expression level among 6 adipose depots

3.5.4 Adipose-enriched miRNAs were implicated in inflammation

Besides its function in metabolism, adipose tissues have emerged as an endocrine organ and an immune organ. Adipose tissues secrete and release hormones, cytokines, chemokines, and growth factors, which mediate and trigger inflammatory response and innate immunity (90). Obesity, which is a state with excessive accumulation of adipose tissue, is recognized as low-grade chronic inflammation (91).

We thus set out to explore the function of adipose-enriched miRNAs in inflammation and immune-mediated disorders. First of all, we found that three major miRNAs which were induced by inflammatory conditions in previous published studies, including miR-21, miR-146 and miR-155, were enriched in adipose tissues (92). miR-21 was determined to be upregulated in psoriasis skin and asthma lung/leukocytes (92). miR-146 and miR-155 was both reported be increased in synovial fibroblasts and peripheral blood mononuclear cells in

rheumatoid arthritis patients. miR-146 also increased in psoriasis skin (92). Their high expression provided evidence to the inflammatory microenvironment of adipose tissues.

Moreover, we found that expression of miR-146 and miR-155 was dependent on particular adipose depot and function, while miR-21 was ubiquitously abundant in all six adipose depots. miR-146 was more enriched in greater omentum and retroperitoneal adipose, while it has a relative low expression in upper layer and inner layer of back fat. miR-155 was more enriched in mesenteric adipose and was relatively low expressed in the other five adipose depots (Table 3.6). Adipose tissues, based on their anatomic location, are classified as SAT and VAT. SAT is found just beneath the skin while VAT is located in abdomen or surrounds vital internal organs such as stomach, liver, and kidney. Both types of adipose tissues are involved in metabolism; however VAT are emphasized for their role in inflammatory processes which precede the development of insulin resistance, type 2 diabetes and cardiovascular complications (93).

To conclude, we demonstrated that pivotal inflammation-induced miRNAs: miR-21, miR-146, and miR-155 were all high abundant in adipose tissues compared to in muscle tissues. Based on further classification of SAT and VAT, miR-146 and miR-155 were more enriched in VAT compared to SAT, while there was no discrepancy on the distribution and expression of miR-21 among different adipose tissues.

3.5.5 Adipose-enriched miRNAs were reported to be oncogenic and they shared common biological pathways with breast cancer overexpressed miRNAs

Strikingly, a large portion (16 out of 29, besides the 3 let-7 family miRNAs) of adipose-enriched miRNAs were also overrepresented in various types of cancers; and their overexpression promotes cancer development, invasion, and metastasis, For instance, besides the well-known oncomiR miR-21, we found miR-103/107, which were overexpressed in gastric cancer and promoted cancer invasion and metastasis, were of high frequency in adipose tissues (94, 95). A list of adipose-enriched miRNAs which possess oncogenic potential in other

tissues and were determined to be of high expression in cancers was presented in Table 3.7.

Instead of functioning individually, multiple miRNAs may work in a coordinate manner to regulate target genes in a common pathway (96, 97). Therefore, pathway enrichment analysis for a set of miRNAs rather than characterization individually will predict the global impact of them on pathways. To evaluate the putative affected pathways by adipose-enriched miRNAs, we carried out miRFocus pathway enrichment analysis. The set of 32 adipose-enriched miRNAs were taken as input query. The majority of miRNAs, 28 out of 32, were associated with target genes, while 4 of them (miR-103a, miR-122, miR-320b, and miR-320d) were not predicted or verified with any target according to the database search. Particularly, the top three miRNAs with highest number of target gene annotations were let-7b, miR-200b, and miR-203 (664, 626, and 535 target annotations, respectively) (Table 3.8).

Eventually, by evaluating *p*-value generated from Fisher's exact test, 36 KEGG pathways were enriched for the set of adipose-enriched miRNAs ($p<0.01$).

Pathway enrichment analysis was also carried out on breast cancer over expressed miRNAs we identified by microarray study. The 22 breast cancer overexpressed miRNAs were subjected to pathway enrichment analysis (Table 3.9). 36 pathways were enriched among the predicted targets from 32 adipose-enriched miRNAs while 19 pathways were enriched from the 22 breast cancer overexpressed miRNAs (Table 3.9).

Interestingly, we found that targets of adipose-enriched miRNAs shared a great portion of enriched pathways with those of breast cancer overexpressed miRNAs. Out of 19 pathways enriched from breast cancer miRNAs, 17 (~90%) pathways were also found enriched in adipose miRNAs. Unique pathways specifically enriched with adipose miRNAs were ErbB signaling pathway and insulin signaling pathway; whereas with breast cancer miRNAs, it was p53 pathway (89, 98-101). p53 pathway serves to guard the cell cycle and its dysfunction leads to cell cycle dysregulation, tumor initiation, and progression (100-103). The ErbB pathway is recognized as oncogenic, controlling cell proliferation, survival, migration, and invasion; while a recent investigation demonstrated its novel role in regulating adipogenesis through ErbB2-FASN axis in adipocytes (99). Insulin

signaling pathway is of pivotal importance in glucose metabolism and lipid metabolism as well as in cell apoptosis, proliferation, and differentiation (104-106). Essential biological pathways, for instance, MAPK pathway, TGF-β pathway, and neurotrophin pathway, were predicted to be affected by both sets of miRNAs (107-109) (Table 3.9).

Overall, pathway enrichment analysis complements miRNA profile analysis and further serves as an innovative approach to discriminate miRNA expression traits and their global biological impacts under different biological systems. The similarity and discrepancy, on the pathway level, between adipose-enriched miRNAs versus breast cancer overexpressed miRNAs, suggested another potential access to explain the rise of obesity to cancer risk.

Limitations of our pathway enrichment analysis included that we did not differentiate either tissue-specific gene expression/function or tissue-specific miRNA-target interactions between adipose tissue and breast cancer samples.

Table 3.7: Adipose-enriched miRNAs were reported to be oncogenic

Adundant miRNAs in adipose tissues	Oncogenesis in cancer
miR-21	breast cancer (Yan et al., 2008), lung cancer (Seike et al., 2009), glioma (Yan et al., 2011), gastric cancer (Zhang et al., 2008), pancreatic cancer (Dillhoff et al., 2008), prostate cancer (Folini et al., 2010), tongue squamous cell carcinoma (Li et al., 2009)
miR-100	prostate cancer (Leite et al., 2011)
miR-103a	esophageal squamous cell carcinoma (Guo et al., 2008), lung cancer (Leidinger et al., 2012), pancreatic tumor (Roldo et al., 2006), gastric cancer (Tchernitsa et al., 2010)
miR-107	breast cancer (Chen et al., 2011), colon cancer (Wentz-Hunter and Potashkin, 2011), gastric cancer (Li et al., 2011)
miR-122	breast cancer (Wu et al., 2012), clear cell renal cell carcinoma (White et al., 2011)
miR-130	lung cancer (Enfield et al., 2011)
miR-140	osteosarcoma (Lulla et al., 2011), lung squamous cell Carcinoma (Tan et al., 2011)
miR-146	papillary thyroid carcinoma, breast cancer, cervical cancer (Rusca and Monticelli, 2011)
miR-148	gastric cancer (Guo et al., 2011), prostate cancer (Murata et al., 2012)
miR-155	lung cancer (Yanaihara et al., 2006), breast cancer (Jiang et al., 2010), pancreatic cancer (Yu et al., 2012), hepatocellular carcinoma (Xiang et al., 2011),
miR-199	hepatocellular carcinoma (Murakami et al., 2011)
miR-221	prostate cancer (Mercatelli et al., 2008), glioma(Zhang et al., 2010), pancreatic cancer (Lee et al., 2007), liver cancer (Pineau et al., 2010), thyroid papillary carcinomas (Visone et al., 2007)

Table 3.8: Putative target genes of adipose-enriched or breast cancer overexpressed miRNAs

Putative target genes of adipose-enriched miRNA		Putative target genes of breast cancer overexpressed miRNA	
miRNA ID	# of target genes	miRNA ID	# of target genes
hsa-let-7b	664	hsa-miR-16	772
hsa-miR-200b	626	hsa-miR-23b	645
hsa-miR-203	535	hsa-miR-200b	626
hsa-let-7c	527	hsa-miR-195	579
hsa-let-7i	515	hsa-miR-200a	478
hsa-miR-200a	478	hsa-miR-26a	448
hsa-miR-130a	451	hsa-miR-107	435
hsa-miR-107	435	hsa-let-7d	416
hsa-miR-155	419	hsa-miR-301a	311
hsa-miR-145	349	hsa-miR-21	281
hsa-miR-148a	346	hsa-miR-425	122
hsa-miR-152	340	hsa-miR-342-3p	86
hsa-miR-21	281	hsa-miR-193a-3p	74
hsa-miR-185	235	hsa-miR-324-5p	60
hsa-miR-221	218	hsa-miR-345	55
hsa-miR-143	179	hsa-miR-193a-5p	54
hsa-miR-199a-3p	173	hsa-miR-191	40
hsa-miR-199b-3p	173	hsa-miR-99a	28
hsa-miR-146a	152	hsa-miR-663	23
hsa-miR-140-3p	137	hsa-miR-615-3p	4
hsa-miR-199a-5p	127		
hsa-miR-122	113		
hsa-miR-146b-5p	86		
hsa-miR-193a-3p	74		
hsa-miR-193a-5p	54		
hsa-miR-100	38		
hsa-miR-375	37		
hsa-miR-199b-5p	25		

Note: Number of target genes was estimated from those have been verified experimentally or those have been commonly predicted with 3 algorisms which were provided in method

Table 3.9: KEGG pathways enriched by adipose-enriched or breast cancer overexpressed miRNAs

Adipose miRNA enriched pathways (36)		
KEGG ID	-Log10(p-value)	KEGG Pathway Description
hsa05200	9.28	Pathways in cancer
hsa04010	7.30	MAPK signaling pathway
hsa04722	6.82	Neurotrophin signaling pathway
hsa05212	6.46	Pancreatic cancer
hsa04012	6.20	ErbB signaling pathway
hsa05220	6.14	Chronic myeloid leukemia
hsa05215	5.77	Prostate cancer
hsa05214	5.48	Glioma
hsa05211	5.15	Renal cell carcinoma
hsa04910	5.10	Insulin signaling pathway
hsa05223	4.59	Non-small cell lung cancer
hsa04510	4.46	Focal adhesion
hsa05210	4.42	Colorectal cancer
hsa04620	4.07	Toll-like receptor signaling pathway
hsa04520	4.07	Adherens junction
hsa04912	3.83	GnRH signaling pathway
hsa05222	3.83	Small cell lung cancer
hsa04621	3.51	NOD-like receptor signaling pathway
hsa04150	3.04	mTOR signaling pathway
hsa05218	2.88	Melanoma
hsa04350	2.88	TGF-beta signaling pathway
hsa05213	2.75	Endometrial cancer
hsa04920	2.70	Adipocytokine signaling pathway
hsa04144	2.63	Endocytosis
hsa04666	2.56	Fc gamma R-mediated phagocytosis
hsa04360	2.48	Axon guidance
hsa04310	2.37	Wnt signaling pathway
hsa04370	2.33	VEGF signaling pathway
hsa05221	2.32	Acute myeloid leukemia
hsa05410	2.18	Hypertrophic cardiomyopathy (HCM)
hsa05219	2.16	Bladder cancer
hsa04664	2.15	Fc epsilon RI signaling pathway
hsa04622	2.14	RIG-I-like receptor signaling pathway
hsa04916	2.09	Melanogenesis
hsa04710	2.03	Circadian rhythm - mammal
hsa04540	2.03	Gap junction

Breast cancer miRNA enriched pathways (19)		
KEGG ID	-Log10(p-value)	KEGG Pathway Description
hsa04010	6.65	MAPK signaling pathway
hsa05200	4.68	Pathways in cancer
hsa05215	4.02	Prostate cancer
hsa05210	4.00	Colorectal cancer
hsa04115	3.26	p53 signaling pathway
hsa05211	3.24	Renal cell carcinoma
hsa05218	3.15	Melanoma
hsa04350	3.14	TGF-beta signaling pathway
hsa04510	3.03	Focal adhesion
hsa04310	2.91	Wnt signaling pathway
hsa04722	2.68	Neurotrophin signaling pathway
hsa04520	2.64	Adherens junction
hsa05214	2.62	Glioma
hsa05220	2.59	Chronic myeloid leukemia
hsa05212	2.40	Pancreatic cancer
hsa05219	2.26	Bladder cancer
hsa04720	2.19	Long-term potentiation
hsa05223	2.04	Non-small cell lung cancer
hsa04144	2.02	Endocytosis

3.6 Conclusion

Altogether, we identified a set of adipose-enriched miRNAs after systematic screening of porcine adipose tissues. We found that adipose-enriched miRNAs were reported to play multiple roles in metabolism, inflammatory processes, and tumorigenesis. The predicted targets of adipose-enriched miRNAs shared a great portion of KEGG pathways with those of breast cancer overexpressed miRNAs, which suggested a possible positive correlation between obesity and cancer risk on the level of signaling cascades. Particular target genes and biological function of adipose-enriched miRNAs await further thorough investigation. Our study provided opportunities to elucidate mechanisms underlying the molecular link between accumulated body mass (obesity), inflammation, and cancer at the miRNA level and highlighted the significance of miRNA functional investigation at the pathway level. Pigs, as an emerging model system, showed a high degree of conservation to humans based on miRNA sequences and expression patterns. Thus, the use of pigs as a model has great potential to benefit biological and medical research as well as therapeutic intervention.

–

Chapter 4: General Discussion and Perspective

–

My dissertation built up as my knowledge accumulated in the miRNA field. There is an on-going explosion of miRNA information nowadays. MiRBase version 18, which has been released in November 2011, contains 18,226 entries representing precursor miRNAs, that express 21,643 mature miRNAs in 168 species. Compared to version 10, which was released in August 2007, the number of entries for miRNAs has increased 3 times.

With the aid of high definition miRNA microarray, we are able to profile the expression of known miRNAs in a fast and convenient way. Newly developed next generation sequencing allows us to access the novel miRNAs as well as other non-coding RNAs, such as long non-coding RNAs and PIWI-interacting RNAs.

Advanced technologies enable the high-throughput screening of miRNAome, even transcriptome, in our samples. However, the understanding of regulation by and of miRNAs, especially the in-depth characterization of each specific miRNA in a temporal and spatial manner, is lacking far behind. A variety of miRNA target

prediction tools have been established and published. Meanwhile, only a small portion, less than 1% of the targets have been experimentally verified.

To study the consequences of excess endogenous prostaglandin E2 (PGE2) in prostate cancer cells (PC-3), I concurrently profiled miRNA and mRNA expression in the same context. Then with the combination of experimental data and computational target prediction, I identified putative miRNA-target mRNA pairs. Furthermore, I identified the candidate networks/pathways which may have been disturbed by the action of PGE2. This approach provided us a new access to determine putative miRNA:mRNA pairs and to better predict biological pathways affected by them.

Another critical feature of miRNAs is that instead of functioning individually, multiple miRNAs may work in concert to regulate their target genes connected by common pathways. This feature enhances the challenges in miRNA functional study and emphasizes the need to evaluate their integrative function on the level of signaling pathways. Thus, in chapter 3, I applied miRFocus, an in-house developed web tool for miRNA pathway enrichment analysis, to better predict the

overall impact of a set of adipose-enriched miRNAs. From there, I was able to interpret which aspects the miRNAs may affect in a broader view.

miRNAs have great potential to become diagnostic targets because of their temporal, spatial, and cell-type specific expression. Meanwhile, miRNA-based therapies, the most challenging and also the most active field, are under development by numerous pharmaceutical companies across the world. The main impediment to this progress is miRNA intracellular delivery, while the second difficulty is evaluation of miRNA-drug efficacy in human clinical trials. To date, quite a few miRNA-drugs are in preclinical stage and a miR-122 targeted drug, which can treat patients with Hepatitis C virus infection, has entered phase II clinical trial. It is hoped that by understanding and validating miRNA expression, their targets, and their function in different diseases, we can use miRNA-based drugs to conquer them.

REFERENCES

1. Jacquier A. The complex eukaryotic transcriptome: unexpected pervasive transcription and novel small RNAs. Nat Rev Genet 2009; 10: 833-44.

2. Esteller M. Non-coding RNAs in human disease. Nat Rev Genet 2011; 12: 861-74.

3. Eddy SR. Non-coding RNA genes and the modern RNA world. Nat Rev Genet 2001; 2: 919-29.

4. Matera AG, Terns RM, Terns MP. Non-coding RNAs: lessons from the small nuclear and small nucleolar RNAs. Nat Rev Mol Cell Biol 2007; 8: 209-20.

5. Kim VN. Small RNAs just got bigger: Piwi-interacting RNAs (piRNAs) in mammalian testes. Genes & Development 2006; 20: 1993-7.

6. Wilusz JE, Sunwoo H, Spector DL. Long noncoding RNAs: functional surprises from the RNA world. Genes & Development 2009; 23: 1494-504.

7. Bartel DP. MicroRNAs: genomics, biogenesis, mechanism, and function. Cell 2004; 116: 281-97.

8. Krol J, Loedige I, Filipowicz W. The widespread regulation of microRNA biogenesis, function and decay. Nat Rev Genet 2010; 11: 597-610.

9. Croce CM. Causes and consequences of microRNA dysregulation in cancer. Nat Rev Genet 2009; 10: 704-14.

10. Streit S, Michalski CW, Erkan M, Kleeff J, Friess H. Northern blot analysis for detection and quantification of RNA in pancreatic cancer cells and tissues. Nat Protoc 2009; 4: 37-43.

11. Pritchard CC, Cheng HH, Tewari M. MicroRNA profiling: approaches and considerations. Nat Rev Genet 2012; 13: 358-69.

12. Trajkovski M, Hausser J, Soutschek J *et al*. MicroRNAs 103 and 107 regulate insulin sensitivity. Nature 2011; 474: 649-53.

13. Fernandez-Hernando C, Suarez Y, Rayner KJ, Moore KJ. MicroRNAs in lipid metabolism. Curr Opin Lipidol 2011; 22: 86-92.

14. Wang T, Li M, Guan J *et al*. MicroRNAs miR-27a and miR-143 Regulate Porcine Adipocyte Lipid Metabolism. Int J Mol Sci 2011; 12: 7950-9.

15. El Ouaamari A, Baroukh N, Martens GA, Lebrun P, Pipeleers D, van Obberghen E. miR-375 targets 3'-phosphoinositide-dependent protein kinase-1 and regulates glucose-induced biological responses in pancreatic beta-cells. Diabetes 2008; 57: 2708-17.

16. Pasquinelli AE. Non-coding RNA MicroRNAs and their targets: recognition, regulation and an emerging reciprocal relationship. Nature Reviews Genetics 2012; 13: 271-82.

17. Wang D, DuBois RN. Prostaglandins and cancer. Gut 2006; 55: 115-22.

18. Karmali RA. Prostaglandins and cancer - Review. Prostaglandins and Medicine 1980; 5: 11-28.

19. Menter DG, Dubois RN. Prostaglandins in cancer cell adhesion, migration, and invasion. Int J Cell Biol; 2012: 723419.

20. Fischer SM. Prostaglandins and cancer. Front Biosci 1997; 2: d482-500.
21. Badawi AF. The role of prostaglandin synthesis in prostate cancer. BJU Int 2000; 85: 451-62.

22. Jain S, Chakraborty G, Raja R, Kale S, Kundu GC. Prostaglandin E2 regulates tumor angiogenesis in prostate cancer. Cancer Res 2008; 68: 7750-9.
23. Sasaki H, Fukushima M. Prostaglandins in the Treatment of Cancer. Anti-Cancer Drugs 1994; 5: 131-8.

24. Hanaka H, Pawelzik SC, Johnsen JI *et al*. Microsomal prostaglandin E synthase 1 determines tumor growth in vivo of prostate and lung cancer cells. Proceedings of the National Academy of Sciences of the United States of America 2009; 106: 18757-62.

25. Lu D, Han C, Wu T. Microsomal prostaglandin E synthase-1 promotes hepatocarcinogenesis through activation of a novel EGR1/beta-catenin signaling axis. Oncogene 2012; 31: 842-57.

26. Bartel DP. MicroRNAs: target recognition and regulatory functions. Cell 2009; 136: 215-33.

27. Kozomara A, Griffiths-Jones S. miRBase: integrating microRNA annotation and deep-sequencing data. Nucleic Acids Res 2011; 39: D152-7.

28. Ruan KH, Cervantes V, So SP. Engineering of a novel hybrid enzyme: an anti-inflammatory drug target with triple catalytic activities directly converting arachidonic acid into the inflammatory prostaglandin E2. Protein Eng Des Sel 2009; 22: 733-40.

29. Buffa FM, Camps C, Winchester L *et al*. microRNA-associated progression pathways and potential therapeutic targets identified by integrated mRNA and microRNA expression profiling in breast cancer. Cancer Res 2011; 71: 5635-45.

30. Gharib SA, Khalyfa A, Abdelkarim A, Bhushan B, Gozal D. Integrative miRNA-mRNA profiling of adipose tissue unravels transcriptional circuits induced by sleep fragmentation. PLoS One 2012; 7: e37669.

31. Steuerwald NM, Parsons JC, Bennett K, Bates TC, Bonkovsky HL. Parallel microRNA and mRNA expression profiling of (genotype 1b) human hepatoma cells expressing hepatitis C virus. Liver Int 2010; 30: 1490-504.

32. Ashburner M, Ball CA, Blake JA *et al*. Gene ontology: tool for the unification of biology. The Gene Ontology Consortium. Nat Genet 2000; 25: 25-9.

33. Lewis BP, Burge CB, Bartel DP. Conserved seed pairing, often flanked by adenosines, indicates that thousands of human genes are microRNA targets. Cell 2005; 120: 15-20.

34. Huang DW, Sherman BT, Lempicki RA. Systematic and integrative analysis of large gene lists using DAVID bioinformatics resources. Nature Protocols 2009; 4: 44-57.

35. Kanehisa M, Goto S. KEGG: kyoto encyclopedia of genes and genomes. Nucleic Acids Res 2000; 28: 27-30.

36. Kanehisa M, Goto S, Sato Y, Furumichi M, Tanabe M. KEGG for integration and interpretation of large-scale molecular data sets. Nucleic Acids Res 2011; 40: D109-14.

37. Wixon J, Kell D. The Kyoto encyclopedia of genes and genomes--KEGG. Yeast 2000; 17: 48-55.

38. Uhlmann S, Zhang JD, Schwager A *et al*. miR-200bc/429 cluster targets PLC gamma 1 and differentially regulates proliferation and EGF-driven invasion than miR-200a/141 in breast cancer. Oncogene 2010; 29: 4297-306.

39. Dohadwala M, Yang SC, Luo J *et al*. Cyclooxygenase-2-dependent regulation of E-cadherin: prostaglandin E(2) induces transcriptional repressors ZEB1 and snail in non-small cell lung cancer. Cancer Res 2006; 66: 5338-45.

40. Brabletz S, Brabletz T. The ZEB/miR-200 feedback loop-a motor of cellular plasticity in development and cancer? Embo Reports 2010; 11: 670-7.

41. Schmalhofer O, Brabletz S, Brabletz T. E-cadherin, beta-catenin, and ZEB1 in malignant progression of cancer. Cancer Metastasis Rev 2009; 28: 151-66.

42. Davies G, Martin TA, Ye L, Lewis-Russell JA, Mason MD, Jiang WG. Phospholipase-C gamma-1 (PLC gamma-1) is critical in hepatocyte growth factor induced in vitro invasion and migration without affecting the growth of prostate cancer cells. Urologic Oncology-Seminars and Original Investigations 2008; 26: 386-91.

43. Sala G, Dituri F, Raimondi C *et al*. Phospholipase C gamma 1 is required for metastasis development and progression. Cancer Research 2008; 68: 10187-96.

44. Maffucci T, Raimondi C, Abu-Hayyeh S *et al*. A phosphoinositide 3-kinase/phospholipase C gamma1 pathway regulates fibroblast growth factor-induced capillary tube formation. PLoS One 2009; 4.

45. Feldman D, Krishnan A, Moreno J, Swami S, Peehl DM, Srinivas S. Vitamin D inhibition of the prostaglandin pathway as therapy for prostate cancer. Nutr Rev 2007; 65: S113-5.

46. Tommasini I, Cerioni L, Palomba L, Cantoni O. Prostaglandin E2 signals monocyte/macrophage survival to peroxynitrite via protein kinase A converging in bad phosphorylation with the protein kinase C alpha-dependent pathway driven by 5-hydroxyeicosatetraenoic acid. J Immunol 2008; 181: 5637-45.

47. Tang CH, Yang RS, Fu WM. Prostaglandin E2 stimulates fibronectin expression through EP1 receptor, phospholipase C, protein kinase Calpha, and c-Src pathway in primary cultured rat osteoblasts. J Biol Chem 2005; 280: 22907-16.

48. Veldman CM, Schlapfer I, Schmid C. Prostaglandin E2 stimulates sodium-dependent phosphate transport in osteoblastic cells via a protein kinase C-mediated pathway. Endocrinology 1998; 139: 89-94.

49. Pai R, Soreghan B, Szabo IL, Pavelka M, Baatar D, Tarnawski AS. Prostaglandin E2 transactivates EGF receptor: a novel mechanism for promoting colon cancer growth and gastrointestinal hypertrophy. Nat Med 2002; 8: 289-93.

50. Wang X, Klein RD. Prostaglandin E2 induces vascular endothelial growth factor secretion in prostate cancer cells through EP2 receptor-mediated cAMP pathway. Mol Carcinog 2007; 46: 912-23.

51. Han C, Michalopoulos GK, Wu T. Prostaglandin E2 receptor EP1 transactivates EGFR/MET receptor tyrosine kinases and enhances invasiveness in human hepatocellular carcinoma cells. J Cell Physiol 2006; 207: 261-70.

52. Buchanan FG, Wang D, Bargiacchi F, DuBois RN. Prostaglandin E2 regulates cell migration via the intracellular activation of the epidermal growth factor receptor. J Biol Chem 2003; 278: 35451-7.

53. Hori R, Nakagawa T, Yamamoto N, Hamaguchi K, Ito J. Role of prostaglandin E receptor subtypes EP2 and EP4 in autocrine and paracrine functions of vascular endothelial growth factor in the inner ear. Bmc Neuroscience 2010; 11.

54. Liu JF, Fong YC, Chang CS *et al*. Cyclooxygenase-2 enhances alpha 2 beta 1 integrin expression and cell migration via EP1 dependent signaling pathway in human chondrosarcoma cells. Molecular Cancer 2010; 9.

55. Tung WH, Hsieh HL, Lee IT, Yang CM. Enterovirus 71 modulates a COX-2/PGE(2)/cAMP-dependent viral replication in human neuroblastoma cells: Role of the c-Src/EGFR/p42/p44 MAPK/CREB signaling pathway. Journal of Cellular Biochemistry 2011; 112: 559-70.

56. Coppola V, De Maria R, Bonci D. MicroRNAs and prostate cancer. Endocr Relat Cancer 2010; 17: F1-17.

57. Lin SL, Chiang A, Chang D, Ying SY. Loss of mir-146a function in hormone-refractory prostate cancer. RNA 2008; 14: 417-24.

58. Pang Y, Young CY, Yuan H. MicroRNAs and prostate cancer. Acta Biochim Biophys Sin (Shanghai) 2010; 42: 363-9.

59. Song Y, Xu Y, Wang Z *et al*. MicroRNA-148b suppresses cell growth by targeting cholecystokinin-2 receptor in colorectal cancer. Int J Cancer 2011.

60. Song YX, Yue ZY, Wang ZN *et al*. MicroRNA-148b is frequently down-regulated in gastric cancer and acts as a tumor suppressor by inhibiting cell proliferation. Molecular Cancer 2011; 10.

61. Kong KL, Kwong DLW, Chan THM *et al*. MicroRNA-375 inhibits tumour growth and metastasis in oesophageal squamous cell carcinoma through repressing insulin-like growth factor 1 receptor. Gut 2012; 61: 33-42.

62. Ding L, Xu YJ, Zhang W *et al*. MiR-375 frequently downregulated in gastric cancer inhibits cell proliferation by targeting JAK2. Cell Research 2010; 20: 784-93.

63. Chang Y, Yan W, He X *et al*. miR-375 inhibits autophagy and reduces viability of hepatocellular carcinoma cells under hypoxic conditions. Gastroenterology 2012.

64. Kinoshita T, Nohata N, Yoshino H *et al*. Tumor suppressive microRNA-375 regulates lactate dehydrogenase B in maxillary sinus squamous cell carcinoma. Int J Oncol 2011; 40: 185-93.

65. Nohata N, Hanazawa T, Kikkawa N *et al*. Tumor suppressive microRNA-375 regulates oncogene AEG-1/MTDH in head and neck squamous cell carcinoma (HNSCC). J Hum Genet 2011; 56: 595-601.

66. Xie H, Sun L, Lodish HF. Targeting microRNAs in obesity. Expert Opin Ther Targets 2009; 13: 1227-38.

67. Khandekar MJ, Cohen P, Spiegelman BM. Molecular mechanisms of cancer development in obesity. Nat Rev Cancer 2011; 11: 886-95.

68. Derdemezis CS, Voulgari PV, Drosos AA, Kiortsis DN. Obesity, adipose tissue and rheumatoid arthritis: coincidence or more complex relationship? Clinical and Experimental Rheumatology 2011; 29: 712-27.

69. Stavropoulos-Kalinoglou A, Metsios GS, Koutedakis Y, Kitas GD. Obesity in rheumatoid arthritis. Rheumatology 2011; 50: 450-62.

70. Sharbati S, Friedlander MR, Sharbati J *et al*. Deciphering the porcine intestinal microRNA transcriptome. BMC Genomics 2010; 11: 275.

71. Li M, Xia Y, Gu Y *et al*. MicroRNAome of porcine pre- and postnatal development. PLoS One 2010; 5: e11541.

72. Zhou X, Zhu Q, Eicken C *et al*. MicroRNA profiling using microParaflo microfluidic array technology. Methods Mol Biol 2012; 822: 153-82.

73. Li M, Liu Y, Wang T *et al*. Repertoire of porcine microRNAs in adult ovary and testis by deep sequencing. Int J Biol Sci 2011; 7: 1045-55.

74. Enright AJ, John B, Gaul U, Tuschl T, Sander C, Marks DS. MicroRNA targets in Drosophila. Genome Biol 2003; 5: R1.

75. Wang X, El Naqa IM. Prediction of both conserved and nonconserved microRNA targets in animals. Bioinformatics 2008; 24: 325-32.

76. Wang X. miRDB: a microRNA target prediction and functional annotation database with a wiki interface. RNA 2008; 14: 1012-7.

77. Krek A, Grun D, Poy MN *et al*. Combinatorial microRNA target predictions. Nat Genet 2005; 37: 495-500.

78. Lall S, Grun D, Krek A *et al*. A genome-wide map of conserved microRNA targets in C. elegans. Curr Biol 2006; 16: 460-71.

79. Maragkakis M, Alexiou P, Papadopoulos GL *et al*. Accurate microRNA target prediction correlates with protein repression levels. BMC Bioinformatics 2009; 10: 295.

80. Maragkakis M, Reczko M, Simossis VA *et al*. DIANA-microT web server: elucidating microRNA functions through target prediction. Nucleic Acids Res 2009; 37: W273-6.

81. Xiao F, Zuo Z, Cai G, Kang S, Gao X, Li T. miRecords: an integrated resource for microRNA-target interactions. Nucleic Acids Res 2009; 37: D105-10.

82. Jiang Q, Wang Y, Hao Y *et al*. miR2Disease: a manually curated database for microRNA deregulation in human disease. Nucleic Acids Res 2009; 37: D98-104.

83. Vergoulis T, Vlachos IS, Alexiou P *et al*. TarBase 6.0: capturing the exponential growth of miRNA targets with experimental support. Nucleic Acids Res 2011; 40: D222-9.

84. Hsu SD, Lin FM, Wu WY *et al*. miRTarBase: a database curates experimentally validated microRNA-target interactions. Nucleic Acids Res 2011; 39: D163-9.

85. Cho IS, Kim J, Seo HY *et al*. Cloning and characterization of microRNAs from porcine skeletal muscle and adipose tissue. Mol Biol Rep 2010; 37: 3567-74.

86. Xie SS, Li XY, Liu T, Cao JH, Zhong Q, Zhao SH. Discovery of porcine microRNAs in multiple tissues by a Solexa deep sequencing approach. PLoS One 2011; 6: e16235.

87. Kim HJ, Cui XS, Kim EJ, Kim WJ, Kim NH. New porcine microRNA genes found by homology search. Genome 2006; 49: 1283-6.

88. Trayhurn P. Adipose tissue in obesity--an inflammatory issue. Endocrinology 2005; 146: 1003-5.

89. Summers SA, Whiteman EL, Birnbaum MJ. Insulin signaling in the adipocyte. Int J Obes Relat Metab Disord 2000; 24 Suppl 4: S67-70.

90. Ouchi N, Parker JL, Lugus JJ, Walsh K. Adipokines in inflammation and metabolic disease. Nat Rev Immunol 2011; 11: 85-97.

91. Wellen KE, Hotamisligil GS. Obesity-induced inflammatory changes in adipose tissue. J Clin Invest 2003; 112: 1785-8.

92. Sonkoly E, Pivarcsi A. microRNAs in inflammation. Int Rev Immunol 2009; 28: 535-61.

93. Li M, Wu H, Wang T *et al*. Co-methylated genes in different adipose depots of pig are associated with metabolic, inflammatory and immune processes. Int J Biol Sci 2012; 8: 831-7.

94. Selcuklu SD, Donoghue MT, Spillane C. miR-21 as a key regulator of oncogenic processes. Biochem Soc Trans 2009; 37: 918-25.

95. Moncini S, Salvi A, Zuccotti P *et al*. The role of miR-103 and miR-107 in regulation of CDK5R1 expression and in cellular migration. PLoS One 2011; 6: e20038.

96. Zhou L, Chen J, Li Z *et al*. Integrated profiling of microRNAs and mRNAs: microRNAs located on Xq27.3 associate with clear cell renal cell carcinoma. PLoS One 2010; 5: e15224.

97. Chen HC, Chen GH, Chen YH *et al*. MicroRNA deregulation and pathway alterations in nasopharyngeal carcinoma. Br J Cancer 2009; 100: 1002-11.

98. Choi SM, Tucker DF, Gross DN *et al*. Insulin regulates adipocyte lipolysis via an Akt-independent signaling pathway. Mol Cell Biol 2010; 30: 5009-20.

99. Vazquez-Martin A, Ortega-Delgado FJ, Fernandez-Real JM, Menendez JA. The tyrosine kinase receptor HER2 (erbB-2): from oncogenesis to adipogenesis. J Cell Biochem 2008; 105: 1147-52.

100. Stegh AH. Targeting the p53 signaling pathway in cancer therapy - the promises, challenges and perils. Expert Opin Ther Targets 2012; 16: 67-83.

101. Sherr CJ, McCormick F. The RB and p53 pathways in cancer. Cancer Cell 2002; 2: 103-12.

102. Udayakumar T, Shareef MM, Diaz DA, Ahmed MM, Pollack A. The E2F1/Rb and p53/MDM2 pathways in DNA repair and apoptosis: understanding the crosstalk to develop novel strategies for prostate cancer radiotherapy. Semin Radiat Oncol 2010; 20: 258-66.

103. Radpour R, Barekati Z, Haghighi MM *et al*. Correlation of telomere length shortening with promoter methylation profile of p16/Rb and p53/p21 pathways in breast cancer. Mod Pathol 2010; 23: 763-72.

104. Liu Q, Gauthier MS, Sun L, Ruderman N, Lodish H. Activation of AMP-activated protein kinase signaling pathway by adiponectin and insulin in mouse adipocytes: requirement of acyl-CoA synthetases FATP1 and Acsl1 and association with an elevation in AMP/ATP ratio. FASEB J 2010; 24: 4229-39.

105. Pereira RI, Draznin B. Inhibition of the phosphatidylinositol 3'-kinase signaling pathway leads to decreased insulin-stimulated adiponectin secretion from 3T3-L1 adipocytes. Metabolism 2005; 54: 1636-43.

106. Yamada T, Katagiri H, Asano T *et al*. Role of PDK1 in insulin-signaling pathway for glucose metabolism in 3T3-L1 adipocytes. Am J Physiol Endocrinol Metab 2002; 282: E1385-94.

107. Bost F, Aouadi M, Caron L, Binetruy B. The role of MAPKs in adipocyte differentiation and obesity. Biochimie 2005; 87: 51-6.

108. Choy L, Skillington J, Derynck R. Roles of autocrine TGF-beta receptor and Smad signaling in adipocyte differentiation. J Cell Biol 2000; 149: 667-82.

109. Luo X, Li HX, Liu RX, Wu ZS, Yang YJ, Yang GS. Beta-catenin protein utilized by Tumour necrosis factor-alpha in porcine preadipocytes to suppress differentiation. BMB Rep 2009; 42: 338-43.